Ultraviolet Radiation Drives Emission of ClimateRelevant Gases From Marine Phytoplankton

JGR Biogeosciences

RESEARCH ARTICLE
10.1029/2021JG006345

Ultraviolet Radiation Drives Emission of Climate-Relevant Gases From Marine Phytoplankton

A. R. McLeod[1], T. Brand[2], C. N. Campbell[2], K. Davidson[2], and A. D. Hatton[2,3]

[1]School of GeoSciences, The University of Edinburgh, Edinburgh, UK, [2]Scottish Association for Marine Science (SAMS), Scottish Marine Institute, Oban, UK, [3]National Oceanography Centre, European Way, Southampton, UK

Key Points:

- Ultraviolet radiation drives emission of climate-relevant gases, including methane and nitrous oxide, from marine phytoplankton cells
- Methane was only produced with cells present, whereas nitrous oxide was also produced after phytoplankton cells were removed by filtration
- Global change impacts on phytoplankton blooms may result in increased UV-driven emissions of these climate-relevant gases

Supporting Information:

Supporting Information may be found in the online version of this article.

Correspondence to:

A. R. McLeod,
Andy.McLeod@ed.ac.uk

Citation:

McLeod, A. R., Brand, T., Campbell, C. N., Davidson, K., & Hatton, A. D. (2021). Ultraviolet radiation drives emission of climate-relevant gases from marine phytoplankton. *Journal of Geophysical Research: Biogeosciences*, *126*, e2021JG006345. https://doi.org/10.1029/2021JG006345

Received 26 MAR 2021
Accepted 18 AUG 2021

Abstract

Marine phytoplankton contribute about one half of global primary production and play a key role in global biogeochemical cycles. High cell densities in extensive phytoplankton blooms are expected to be modified by global changes in ocean circulation and stratification, acidification and carbonation, solar radiation, temperature, and eutrophication. Although photochemical gas production from chromophoric dissolved organic matter (CDOM) has been widely studied, ultraviolet (UV) effects on emissions from phytoplankton cells themselves have not been fully explored. We therefore investigated UV-driven emissions of carbon monoxide (CO), carbon dioxide (CO_2), methane (CH_4), ethene (C_2H_4), ethane (C_2H_6), and nitrous oxide (N_2O) from cell suspensions of 16 phytoplankton species and their filtrates under controlled experimental conditions. These gases make direct or indirect contributions to radiative forcing of the atmosphere or contribute to atmospheric chemistry including stratospheric ozone (O_3) depletion. We observed production of CH_4, CO, CO_2, C_2H_4, and N_2O from cell suspensions and CO, CO_2, and N_2O after 0.45 μm-filtration to remove phytoplankton cells. CH_4 production was only observed with cells present, whereas N_2O was still produced after filtration. Production of CO from filtrates was 30%–90% of that from cell suspensions in all but two species with a CO_2:CO mole ratio from filtrates always below one. Our results clearly demonstrate a need to quantify the production potentials of these climate-relevant gases *in situ* under natural sunlight using key phytoplankton species, especially those forming blooms which are predicted to change in prevalence and distribution with future global change scenarios.

Plain Language Summary

The oceans play an important role in the global exchange of gases with the atmosphere including the greenhouse gases carbon dioxide and methane that contribute to global warming. Several recent studies have shown that phytoplankton metabolism can produce methane during growth. Other studies also demonstrated that sunlight can degrade dissolved organic matter and plastic particles in seawater to produce methane and other gases. However, few studies have examined whether the ultraviolet radiation in sunlight can drive production of methane and other climate-relevant gases from the cells of phytoplankton. In this study, we exposed cell suspensions of 16 phytoplankton species to controlled levels of ultraviolet radiation in the laboratory. We observed production of methane, carbon dioxide, carbon monoxide, ethene and also the important greenhouse gas nitrous oxide from cell suspensions. Nitrous oxide was still produced after phytoplankton cells were removed by filtration, whereas methane was only produced with cells present. These gases make direct or indirect contributions to global warming and atmospheric chemistry. Blooms of phytoplankton cells may cover extensive areas of the ocean. Consequently, it is important to evaluate the role of the ultraviolet component of sunlight to emissions of these gases under future global change scenarios.

1. Introduction

Photochemical emissions to the atmosphere from the marine and freshwater environment have recently received attention for their role and contribution to biogeochemical cycles of carbon (Cory et al., 2014; Günthel et al., 2019; Koehler et al., 2014; Li et al., 2020; Neale et al., 2021; Royer et al., 2018). Oxidation of dissolved organic carbon (DOC) by ultraviolet (UV) and visible radiation was reported to contribute 70%–95% of DOC breakdown and 40% of CO_2 emissions in arctic lakes and rivers (Cory et al., 2014). Photochemical processes in seawater are involved in formation of CO_2, CO, carbonyl sulphide (COS), dimethylsulphide (DMS), and alkyl nitrates (Mopper et al., 2015). Additionally, UV-driven production of methane (CH_4), ethene (C_2H_4), and ethane (C_2H_6) were recently reported from plastic particles in seawater (Royer et al., 2018).

No photochemical production of CH_4 was detected from 0.2 μm-filtered estuarine and marine samples by Bange and Uher (2005), but there remains considerable debate about the sources of CH_4, which supersaturates the upper waters of many marine and freshwater systems (Donis et al., 2017; Günthel et al., 2019; Tang et al., 2016). This CH_4 accumulation above atmospheric equilibrium in well-oxygenated surface layers, often termed "the methane paradox," has led to several investigations of oxic CH_4 formation (Tang et al., 2016), including microbial degradation of organic phosphorus compounds (Perez-Coronel & Beman, 2020; Repeta et al., 2016; Sosa et al., 2020) and metabolic production of CH_4 in marine *Cyanobacteria* (Bižić et al., 2020). Althoff et al. (2014) suggested that algae-derived dimethylsulphoxide (DMSO) could be a precursor of CH_4 formation in oxic seawater. CH_4 production in the widespread marine coccolithophore *Emiliania huxleyi* was observed under visible light by Lenhart et al. (2016) and also in the haptophytes *Phaeocystis globosa* and a *Chrysochromulina* sp. by Klintzsch et al. (2019, 2020). These studies all relate CH_4 production with phytoplankton metabolism rather than photochemical transformation of cell components. Most recently, Li et al. (2020) measured CH_4 and CO photoproduction from a range of 0.2 μm-filtered land-ocean water samples, and used a remote sensing-informed photochemical model to conclude that photodegradation of CDOM in the surface ocean is likely an important contributor to the methane paradox.

Most aquatic studies of photochemical gas production have focused on allochthonous DOM in freshwater, estuarine, or coastal environments rather than particulate organic matter (POM) and phytoplankton cells (e.g., Cory et al., 2014; Li et al., 2020; Stubbins et al., 2011; Vachon et al., 2016). However, Wilson et al. (1970) investigated photoproduction of CH_4, CO, and C2–C4 hydrocarbons from autochthonous DOM produced by phytoplankton cultures. They observed no production of CH_4 or higher saturated hydrocarbons, but CO, C_2H_4, and propene (C_3H_6) were produced from cell-free samples when illuminated. McKay et al. (1996) measured emission of 27 non-methane hydrocarbons from axenic cultures of the diatom *Skeletonema costatum* and the dinoflagellate *Scrippsiella trochoidea* illuminated for over 3 months with a fluorescent light source. They suggested that C_2H_4, C_2H_6, C_3H_6, and propane (C_3H_8) were produced from cell autolysis releasing polyunsaturated lipids but reported only isoprene (C_5H_8) and hexane (C_6H_{14}) production from living cells or their exudates. Günthel et al. (2020) reported CH_4 production in oxic lake water associated with phytoplankton photosynthesis and phosphorus metabolism. They also demonstrated production by a freshwater diatom *Navicula* sp. and a marine diatom *Leptocylindrus danicus* that increased at higher visible irradiances, while Hartmann et al. (2020) detected CH_4 production from eight freshwater phytoplankton species.

However, these studies only considered visible radiation, and none investigated the effect of UV radiation on photochemical emissions from phytoplankton or their exudates in marine waters. UV-driven foliar emissions of CO_2, CH_4, C_2H_4, C_2H_6, C_3H_8, and CO were demonstrated in 30 higher plant species by Fraser et al. (2015) and CH_4 emissions observed from several studies of plants and their structural components (Bruhn et al., 2012; Keppler et al., 2006; Vigano et al., 2008). Messenger et al. (2009) suggested that a mechanism for CH_4 production could be the photochemical generation of reactive oxygen species (ROS) in leaves, including the hydroxyl radical (OH). In seawater, sunlight-driven formation of OH and other reactive radicals (e.g., superoxide (O_2^-), hydrogen peroxide (H_2O_2) and singlet oxygen ($^1O_2$)) has also been shown to occur, resulting in the direct and indirect photochemical oxidation of DOM to generate low molecular weight carbonyl molecules, CO and CO_2 (Mopper & Kieber, 2005; Mopper et al., 2015).

Marine DOM is one of the largest global C pools, comprising ~662 ± 32 Pg (10^{15} g) C (Carlson & Hansell, 2015). Terrestrial DOM dominates in coastal and estuarine areas but comprises only 0.7%–2.4% of DOM in the open ocean (Sulzberger & Durisch-Kaiser, 2009), which is mostly composed of autochthonous matter comprising cell detritus or extracellular release by phytoplankton. It is therefore important to understand the UV photochemistry of autochthonous DOM, particularly as phytoplankton blooms are expected to increase with climate change, increased atmospheric CO_2 and ocean acidity (Richardson et al., 2019; Riebesell et al., 2018). Phytoplankton and bacterial cells and detritus are also a key component of POM, which can undergo photochemical modification to DOM and gaseous emissions (Sulzberger et al., 2019). Xie and Zafiriou (2009) demonstrated CO photoproduction from both DOM and POM in filtered and unfiltered samples of open-ocean and coastal waters. In many parts of the surface ocean, dissolved organic nitrogen (DON), generated by phytoplankton and their exudates, is also an important source of nitrogen and a key component of the DOM pool. Although we are not aware of any estimates of photochemical nitrous oxide

(N_2O) formation from marine phytoplankton, UV photoproduction of N_2O from higher plants has been reported (Bruhn et al., 2014).

We therefore investigated if marine phytoplankton cells were a possible source of UV-driven emissions of CO, CO_2, CH_4, C_2H_4, C_2H_6, and N_2O. These gases all play a role in the Earth's energy balance and can contribute directly and indirectly to positive radiative forcing. CO_2, CH_4, and N_2O are greenhouse gases, while CO reacts to reduce atmospheric OH that can otherwise oxidize CH_4. CO also contributes to tropospheric O_3 formation, which is also a greenhouse gas, and C_2H_4, and C_2H_6 can react to produce CH_4, CO_2, and O_3 (IPCC, 2013; Sulzberger et al., 2019).

Our experiments were designed to investigate UV-driven emissions from cells of marine and estuarine phytoplankton species and their filtrates in seawater. Sixteen species were chosen for study as representatives of a range of key phytoplankton groups (including chlorophytes, cryptophytes, haptophytes, myzozoans, and ochrophytes) and were investigated by laboratory irradiation of cell cultures and their filtrates.

2. Materials and Methods

2.1. Culture Media and Conditions

Marine phytoplankton were sourced from the UK Culture Collection of Algae and Protozoa (CCAP), Oban, UK and listed in Table 1 with details of their origin. Five of the monospecific algal cultures were axenic while the remainder contained bacterial associates. Isolates were inoculated into three replicate acid-washed 250 ml Erlenmeyer flasks containing 125 ml f/2 + Si medium for diatoms (Guillard & Ryther, 1962) in sterile artificial seawater comprising 33.6 g L^{-1} Ultramarine Synthetica Sea Salt (Waterlife Research Industries Ltd.,

Longford, UK) in ultrapure water (Type 1: resistivity 18.2 MΩ cm) and grown for 10 days under a 12:12 h light:dark cycle at 20°C and irradiance of ~6.6 W m^{-2} (30.9 μmol m^{-2} s^{-1}) PAR (photosynthetically active radiation, 400–700 nm) providing cultures for exposure in the late exponential growth phase. A flask of un-inoculated medium was also maintained under the same conditions to provide control samples.

2.2. Experimental Treatments

The three replicate flasks of each species were combined and then three 60 ml samples filtered through pre-weighed sterile 0.45 μm-pore membrane filters (MF-Millipore™ MCE, Merck Millipore Ltd., Cork, Ireland) to remove phytoplankton cells and provide a filtrate. Three replicate samples of 1 ml were also fixed in 1% Lugols iodine to assess cell numbers. Cells were counted using a Zeiss Axiovert 200 inverted light microscope (Carl Zeiss Ltd., Cambridge, UK) at ×200 magnification. Dinoflagellates, with large cells, were counted using a Sedgewick Rafter counting chamber (Model S52, Graticules Optics Ltd., Tonbridge, Kent, UK) and smaller cells (<15 μm) were counted using an improved Neubauer double cell hemocytometer (Marienfeld Superior 0630010, Fisher Scientific, Loughborough, Leicestershire, UK) assessing a minimum of 200 fields 0.0025 mm^2 × 0.1 mm.

Samples of unfiltered and 0.45 μm-filtered cell suspensions were bubbled with sterile (0.2 μm filtered) ambient air at 60 ml min^{-1} for 30 min in order to equilibrate dissolved gases with ambient concentrations. 15 ml samples were then transferred into standard 20 ml vials (i.d. 1.9 cm) made of UV-transmitting quartz (Robson Scientific, Sawbridgeworth, Hertfordshire, UK) and sealed with Al crimp caps with PTFE-coated silicone septa (Chromacol Type 20-AC-ST3, Thermo Fisher Scientific, Paisley, UK). Tubing, vials, and other glassware were autoclaved before use and sterile technique employed at all times. As vial volume varied slightly, each vial was numbered by engraving on the base and individual volumes determined gravimetrically using water to allow calculation of precise headspace volumes. Three replicate vials of filtered and unfiltered cell suspension were irradiated, and three replicate vials also wrapped in Al foil as dark controls. Two species were studied in each experiment together with three replicate vials of irradiated and un-irradiated artificial seawater and of 20 mg L^{-1} Nordic Aquatic Fulvic Acid (NAFA) reference standard (Nordic Lake Type 1R105 F, International Humic Substances Society, St. Paul, MN, USA). Each experiment also included two replicate vials of irradiated and un-irradiated ultrapure water as control comparisons.

Table 1
Phytoplankton Species Used in This Study, Their Origin, and Mean Cell Number

Phylum	Class	Species	Culture ID	Origin (*axenic culture/bacterial presence*)	Cell number ± 1 s.e(ml^{-1})
Haptophyta	Prymnesiophyceae	*Isochrysis galbana* Parke	CCAP 927/1	Isle of Man, UK. *Axenic culture*	$3.72\ (\pm0.13) \times 10^6$
		Emiliania huxleyi (Lohmann) W. W. Hay & H. P. Mohler	CCAP 920/8	Marine; Bergen, Norway. *Bacteria present*	$2.04\ (\pm0.14) \times 10^5$
		Chrysotila carterae (Braarud & Fagerland) Andersen, Kim, Tittley & Yoon	CCAP 961/8	Brackish pool, Dunstaffnage Castle, Oban, Scotland, UK. *Bacteria present*	$1.76\ (\pm0.15) \times 10^5$
	Pavlovophyceae	*Diacronema lutheri* (Droop) Bendif & Véron	CCAP 931/1	Millport, UK. *Axenic culture*	$3.29\ (\pm0.09) \times 10^6$
Ochrophyta	Eustigmatophyceae	*Nannochloropsis oculata* (Droop) D. J. Hibberd	CCAP 849/1	Skate Point, Isle of Cumbrae, Scotland, UK. *Axenic culture*	$2.73\ (\pm0.87) \times 10^7$
	Raphidophyceae	*Heterosigma akashiwo* (Hada) Hada ex Hara & Chihara	CCAP 934/5	Fidalgo Island, Burrows Bay, Washington, USA. *Bacteria present*	$3.23\ (\pm0.25) \times 10^5$
	Bacillariophyceae	*Skeletonema marinoi* Sarno & Zingone	CCAP 1077/5	Long Island Sound, Milford Harbor, CN, USA. *Bacteria present*	$8.02\ (\pm0.45) \times 10^5$
		Cyclotella cryptica Reimann, Lewin & Guillard	CCAP 1070/2	West Tisbury, Great Pond, Martha's Vineyard, MA, USA. *Bacteria present*	$9.92\ (\pm0.39) \times 10^5$
		Thalassiosira pseudonana Hasle & Heimdal	CCAP 1085/12	Moriches Bay, Forge River, Long Island, NY, USA. *Axenic culture*	$2.83\ (\pm0.06) \times 10^6$
Chlorophyta	Mamiellophyceae	*Micromonas pusilla* (Butcher) Manton & Parke	CCAP 1965/4	English Channel near Plymouth, UK. *Bacteria present*	$1.65\ (\pm0.11) \times 10^7$
	Chlorodendrophyceae	*Tetraselmis tetrathele* (West) Butcher	CCAP 66/35	Rock pool Dunstaffnage, Argyll, Scotland, UK. *Axenic culture*	$1.75\ (\pm0.20) \times 10^5$
Myzozoa	Dinophyceae	*Scrippsiella acuminata* (Ehrenberg) Kretschmann et al.	CCAP 1134/8	Loch Creran, Argyll, Scotland, UK. *Bacteria present*	$9.00\ (\pm0.23) \times 10^2$
		Prorocentrum micans Ehrenberg	CCAP 1136/18	Loch Creran, Argyll, Scotland, UK. *Bacteria present*	$5.75\ (\pm0.39) \times 10^3$
		Alexandrium tamarense (Lebour) Balech	CCAP 1119/1	St Germans River, Tamar Estuary, Cornwall, UK. *Bacteria present*	$6.28\ (\pm0.46) \times 10^2$
		Lingulodinium polyedra (F.Stein) J. D. Dodge	CCAP 1121/2	Loch Creran, Argyll, Scotland, UK. *Bacteria present*	$8.43\ (\pm0.81) \times 10^3$
Cryptophyta	Cryptophyceae	*Rhodomonas atrorosea* Butcher ex Hill & Wetherbee	CCAP 978/6A	Pagham Harbor, Sussex, England, UK. *Bacteria present*	$4.87\ (\pm0.51) \times 10^5$

Note. Species classification according to the World Register of Marine Species (WoRMS) at http://www.marinespecies.org. Further details of source cultures are available from http://www.ccap.ac.uk.

All experiments were performed under oxic conditions, and gas chromatography detected no reduction in headspace oxygen (O_2), which remained >20% at the end of each experiment.

2.3. Ultraviolet Exposure System

Ultraviolet treatments were performed in a black irradiation tank with vials exposed sideways and submerged in flowing water maintained at 20 °C by a re-circulating thermochiller (Model TR15, Teco S.r.l., Ravenna, Italy). Two 40 W Q-Panel 313 fluorescent lamps (The Q-Panel Company, Cleveland, OH, USA) were mounted horizontally inside UV-transparent quartz tubing (44 mm o.d., 2 mm wall thickness; Robson Scientific) running through the tank at 5 cm from the vials. Lamps were wrapped in cellulose diacetate (CA) film (125 μm; Courtaulds Speciality Plastics, Derby, UK) to remove emissions below 290 nm (which do not reach the Earth's surface) to provide a treatment that included UV-B (280–315 nm) and UV-A (315–400 nm)

Table 2
Irradiance and Accumulated Dose of Ultraviolet and Photosynthetically Active Radiation During Exposure

	All UV	UVA	UVB	All PAR	VIO	BLU	CIE	DNA	GEN	PG	PRO	EUK	CH_4	ROS
Energy irradiance (W m^{-2})	8.30	4.31	3.99	1.82	1.21	0.03	1.14	1.87	1.95	1.87	3.44	2.52	5.15	5.27
Photon irradiance (μmol m^{-2} s^{-1})	22.09	11.93	10.16	7.17	4.23	0.13	2.82	4.67	4.86	4.67	8.57	6.28	12.82	13.13
8-h dose (kJ m^{-2})	239.0	124.1	114.9	52.4	34.8	0.9	32.8	53.9	56.2	53.9	99.1	72.6	148.3	151.8

Note. Wavelengths and abbreviations used: All UV (280–400 nm), UVA (315–400), UVB (280–315 nm), All PAR (400–700 nm), VIO (violet: 400–455 nm), and BLU (blue: 455–492 nm), plus weighted UV using a range of common spectral weighting functions: CIE, the Commission Internationale de l'Eclairage erythemal action spectrum (McKinlay & Diffey, 1987; Webb et al., 2011); DNA, the DNA damage action spectrum (Setlow, 1974); GEN, a mathematical function (Green et al., 1974) of the general plant action spectrum (Caldwell, 1971); PG, the plant growth function of Flint and Caldwell (2003); PRO, a function for the mean photosynthetic inhibition of three strains of prokaryotic picophytoplankton at 20°C (Neale & Thomas, 2017); a function for inhibition of photosynthesis in the eukaryotic flagellate *Dunaliella salina* (Ghetti et al., 1999); CH_4, a function for CH_4 production from plant pectins (McLeod et al., 2008); ROS, a function for H_2O_2 production in seawater (Kieber et al., 2014). All weighting functions (except CIE) were normalized to unity at 300 nm and converted from the original published units following the procedures given by Aphalo et al. (2012).

wavelengths. Spectra of CA transmission and CA-filtered lamps are provided by McLeod et al. (2008). Irradiation was continuously measured with a broad-band sensor (Model PMA2102; Solar Light Inc., Glenside, PA, USA) inside a black waterproof housing at 5 cm distance behind a quartz window of the same thickness as the wall of quartz vials. Lamp output was adjusted by PC-based software to maintain a constant irradiance and compensate for any change in transmittance of the CA-filters. The broad band sensor was calibrated with a double monochromator spectroradiometer (SR991-PC, Macam Photometrics, Livingston, West Lothian, UK) itself calibrated against a tungsten and deuterium lamp traceable to UK National Physical Laboratory Standards (SR903, Macam Photometrics). The UV treatment was a constant 8-h irradiance of 8.3 W m^{-2} unweighted UV (comprising 4.31 W m^{-2} UVA and 3.99 W m^{-2} UVB), which was 1.14 W m^{-2} of UV weighted with the erythemal action spectrum, which is typically used to report global levels of UV (McKinlay & Diffey, 1987; Webb et al., 2011). This irradiance allowed detection of changes in headspace concentrations while ensuring minimal depletion of O_2. The irradiance and accumulated 8-h dose of PAR and UV, calculated using a range of common spectral weighting functions, are given in Table 2 (as recommended by Aphalo et al., 2012) including examples from the marine environment for inhibition of photosynthesis in prokaryotic and eukaryotic marine phytoplankton, production of the reactive oxygen species H_2O_2 in seawater, and photochemical production of CH_4 from plant pectins. The photon irradiance and accumulated dose are included to facilitate comparison with published work including widely reported global values of daily dose from sunlight exposure measured in kJ m^{-2}.

Actinometric measurements were also performed in order to quantify the UV photon fluence inside the quartz vials, using a standard ferrioxalate actinometer method (Aphalo et al., 2012) with all exposures and reagent preparation performed in darkness or under red light (>600 nm). Three replicate quartz vials containing 15 ml of freshly prepared 0.006 M potassium trisoxalatoferrate(III) trihydrate (Chemos GmbH, Regenstauf, Germany) were irradiated for durations between zero and 3 min using the same radiation geometry as the cultures. Vials were pulled into opaque black tubes after each interval and stored in darkness before analysis using 1,10 phenanthroline monohydrate (Sigma-Aldrich Chemical Co., Poole, UK) and sodium acetate buffer according to Aphalo et al. (2012). Formation of Fe^{2+} was measured by absorbance at 510 nm (A_{510}) with a Jenway 7315 spectrophotometer (Bibby Scientific Ltd., Stone, UK), exactly 30 min after reagent addition, using unexposed ferrioxalate solution as a blank.

2.4. Gas Chromatography and Partition Calculations

Concentrations of CO, CO_2, CH_4, C_2H_4, C_2H_6, N_2O, and O_2 in vial headspace were measured with an Agilent 6890 gas chromatograph (GC) (Agilent Technologies, Wilmington, DE, USA), equipped with an HT200H headspace autosampler (HTA s.r.l., Brescia, Italy). The carrier gas of O_2-free N_2 (BOC Special Gases, Guildford, Surrey, UK) was filtered with a hydrocarbon trap (Type 14633, Alltech Associates Inc., IL, USA), a custom made CO_2 scrubber filled with self-indicating 1.0–2.5 mm NaOH granules (*Sofnolime*, Molecular Products Inc., Boulder, CO, USA), a moisture filter (*Hydropurge* II, Alltech Associates Inc.), and an inert gas filter (Gatekeeper Type CE500KFI4R, Entegris Inc., Billerica, MA, USA). The N_2 carrier flow of 45 ml

min^{-1} was split between two separate column pathways. One pathway comprised a methanizer (to allow CO and CO_2 measurement) followed by a 0.3 m length packed column (Hayesep-D, 80–100 mesh, HaySeparations Inc., TX, USA) in series with a 3 m length molecular sieve (Type 13X, 80/100 mesh, 2 mm i.d., Agilent Technologies). These supplied a flame ionisation detector (FID) held at 250°C for measurement of CO, CO_2, CH_4, C_2H_4, C_2H_6, and O_2. The second pathway comprised 2 m of 0.32 mm i.d. methyl-deactivated fused silica capillary column with no stationary phase supplying an electron capture detector held at 350°C for measurement of N_2O and O_2. Gas flows between the packed column, molecular sieve, and FID used a ten-port switching valve (Valco Instrument Co. Inc., Houston, TX, USA) that allowed reversal of the FID column sequence during the run after 1.6 min, so that CO_2 passed directly to the detector from the packed column while CO and O_2, which would otherwise elute together, were separated by the molecular sieve and re-circulated through the packed column a second time. The total carrier flow was reduced by 4 ml min^{-1} between 1.6 and 2.3 min in order to optimize peak separation. Analytical runs lasted 8 min, comprising an isothermal period at 65°C for 2.3 min, followed by an increase of 60°C min^{-1} to 92°C held for 1.8 min. Oven temperature was then decreased by 60°C min^{-1} during the remainder of the run to the initial oven temperature. A 2.5 ml autosampler syringe removed 2 ml from each vial headspace and injected through a PTFE-coated silicone septum (GP septum type 041825, SGE Analytical Science Pty Ltd, Australia) to fill a 1 ml sample loop that was automatically switched into the carrier flow after 0.1 s to allow equalization of the loop to atmospheric pressure. Peak integration was performed by Clarity Chromatography Software Ver. 3.0.07.662 (DataApex Ltd., Prague, Czech Republic). Atmospheric pressure was recorded daily by Oban Airport Weather Station (UK Grid Reference NM908355), 2.8 km from the laboratory (Worldwide Weather Online, 2019) and used in calculation of gas partition.

Calibration of GC response was performed during each experiment using three replicate injections of carrier N_2 and 100%, 50% and 25% dilutions of a mixed standard of seven gases in synthetic air (20.8% O_2) comprising CO_2 1541 ppm, CO 20.1 ppm, CH_4 3.18 ppm, C_2H_4 20.8 ppm, C_2H_6 20.8 ppm, and N_2O 4.86 ppm (BOC Special Gases). The standard deviation of the mean of six samples of the standard gas was below 1.0%, 1.2%, 1.3%, 5.0%, 1.1%, and 2.0% for CO_2, CO, CH_4, C_2H_4, C_2H_6, and N_2O respectively.The mass of each gas (m_{gas}) in vial headspace was calculated from the ideal gas law (Equation 1),

$$m_{gas} = \frac{P \times V}{R \times T} \times M_{gas} \times C_{gas}, \quad (1)$$

where P = pressure, V = volume, R = ideal gas constant, T = temperature, C_{gas} = mixing ratio, and M_{gas} = molar mass.

The solubility of gases in the water phase and dissolved gas content was calculated from the headspace concentration, headspace volume, temperature, salinity, and atmospheric pressure according to Wiesenburg and Guinasso (1979) for CH_4 and CO, according to Weiss and Price (1980) for N_2O and CO_2, and according to Breitbarth et al. (2004) for C_2H_4. Total gas production was calculated from the sum of the headspace and dissolved gas content in each vial.

2.5. Dissolved and Particulate Carbon and Nitrogen

Dissolved organic carbon (DOC) and total dissolved nitrogen (TDN) of un-irradiated 0.45 μm-filtered samples (from 10 species only) and un-inoculated artificial seawater was determined at the start of the experiment. The combined analysis system comprised a Shimadzu TOC-VCPH Total Organic Carbon Analyzer (Shimadzu Corporation, Kyoto, Japan) with platinum catalyst (0.5% on alumina), compressed air carrier gas (150 ml min^{-1}) coupled to a Non-Dispersive Infra-Red (NDIR) detector used to determine DOC coupled with a Shimadzu Total Nitrogen Measuring Unit (TNM-1) for determination of TDN by high temperature oxidation to nitric oxide and detection by chemiluminescence (Sharp et al., 2004).

Filtered 20 ml samples were collected in pre-combusted glass ampoules, preserved with 50 μL 85% orthophosphoric acid, and stored at 4–6°C in darkness until analysis. Calibration was performed using a dilution series mixture containing glycine and potassium hydrogen phthalate (Shimadzu Co.). Instrument precision was checked daily using a consensus reference standard (Deep Sea Reference RSMAS/MAC, University of Miami, USA).

Samples of 15 ml cell suspension of the same 10 species were also filtered onto pre-combusted (450°C, 4 h) 25 mm diameter GF/F filters (Whatman Type 1825-025, GE Healthcare Life Sciences, Buckinghamshire, UK) for the analysis of particulate organic C and N (POC and PON). Filters were frozen at −20°C until analysis, acidified overnight under vacuum in a desiccator with concentrated HCl to remove $CaCO_3$, then dried under vacuum with silica gel crystals for 8 h before analysis with a Costech ECS 4010 Elemental Combustion Analyzer (Costech Analytical Technologies Inc., Valencia, CA, USA). Instrument calibration was performed during each run with a range of five weights of acetanilide (C_8H_9NO) and three blanks using an additional C_8H_9NO sample between every 12 experimental samples to monitor for any instrument drift. The limit of detection estimated from three standard deviations of the mean of blank data was 1 μg for both C and N.

2.6. Statistical Analysis

Data for some gaseous emissions were not normally distributed, even after transformation, and three replicate measurements precluded accurate parametric statistical tests between species. The effect of UV irradiance on emissions was therefore tested separately for each gas across all 16 species by the non-parametric Wilcoxon (Matched pairs) Signed Rank test and data plotted with the standard error of the mean to illustrate variation between replicates. The standard errors of mean net emissions were calculated from the difference between irradiated and un-irradiated samples according to Motulsky (1995). Non-parametric Spearman rank correlations (r_s) were calculated between net gas emissions and initial N and C content. All analyses were completed using SigmaPlot version 14 software (Systat Software Inc., San Jose, CA, USA).

3. Results

3.1. Net UV-Driven Gas Production

Net UV-driven gas production from unfiltered and 0.45 μm-filtered cell suspensions (mean of UV-exposed samples minus mean of unexposed samples in the dark) is shown for each species in Figure 1 together with production from ultrapure water, un-inoculated seawater and the NAFA standard. The Signed Rank test revealed significant differences between the gas production from UV-irradiated and un-irradiated samples, for CH_4, CO, N_2O, and C_2H_4 from unfiltered samples and for CO, CO_2, and N_2O from 0.45 μm-filtered samples. There was no detectable production of C_2H_6 from any species. Mean production rates for each gas in molar units and per unit mass of POC are also provided in Table S1. The gas production from cells >0.45 μm in the dark (mean of un-irradiated unfiltered samples minus un-irradiated 0.45 μm-filtered samples) are provided in Table S2 and were significantly different (Signed Rank test, $p < 0.001$, $n = 16$) only for CO_2 and were positive values in all species indicative of respiration. The difference between UV-irradiated values for unfiltered and filtered samples in Figure 1 provide estimates of net UV-driven gas production from cells >0.45 μm only and are also provided in Table S2. These data also indicate a significant difference caused by the presence of cells >0.45 μm (Signed Rank test, $p < 0.001$, $n = 16$) in production of all gases except N_2O.

We considered estimating UV-driven gas production from phytoplankton cells and their filtrates (plus any bacteria in non-axenic cultures) by subtraction of un-inoculated seawater production on irradiation from that of unfiltered and filtered cell suspensions. However, this was not done because the original content of the seawater would have been modified during the 10 days of culture growth prior to irradiation by metabolic activity of the phytoplankton (and any bacterial associates) including any extracellular release of DOC. Such a calculation would have been appropriate if the medium had been inoculated at the start of exposure as undertaken by McKay et al. (1996). Our calculation also corrects for any dark microbial gas production during the exposure period by subtracting production in dark controls from UV-exposed samples. Potential changes in the medium during cell growth prior to irradiation include alkalinity (and pH), which would influence the balance between dissolved CO_2, bicarbonate (HCO_3^-) and carbonate (CO_3^{2-}) to modify CO_2 solubility in particular.

UV irradiation of the NAFA standard produced CO and CO_2 but no detectable CH_4. The Signed Rank test revealed significant differences in CO production caused by UV irradiation of the NAFA standard, un-inoculated seawater and ultrapure water (all $p < 0.01$, $n = 8$) and also in CO_2 production by the NAFA standard and ultrapure water ($p < 0.01$, $n = 8$ and $p < 0.05$, $n = 8$ respectively).

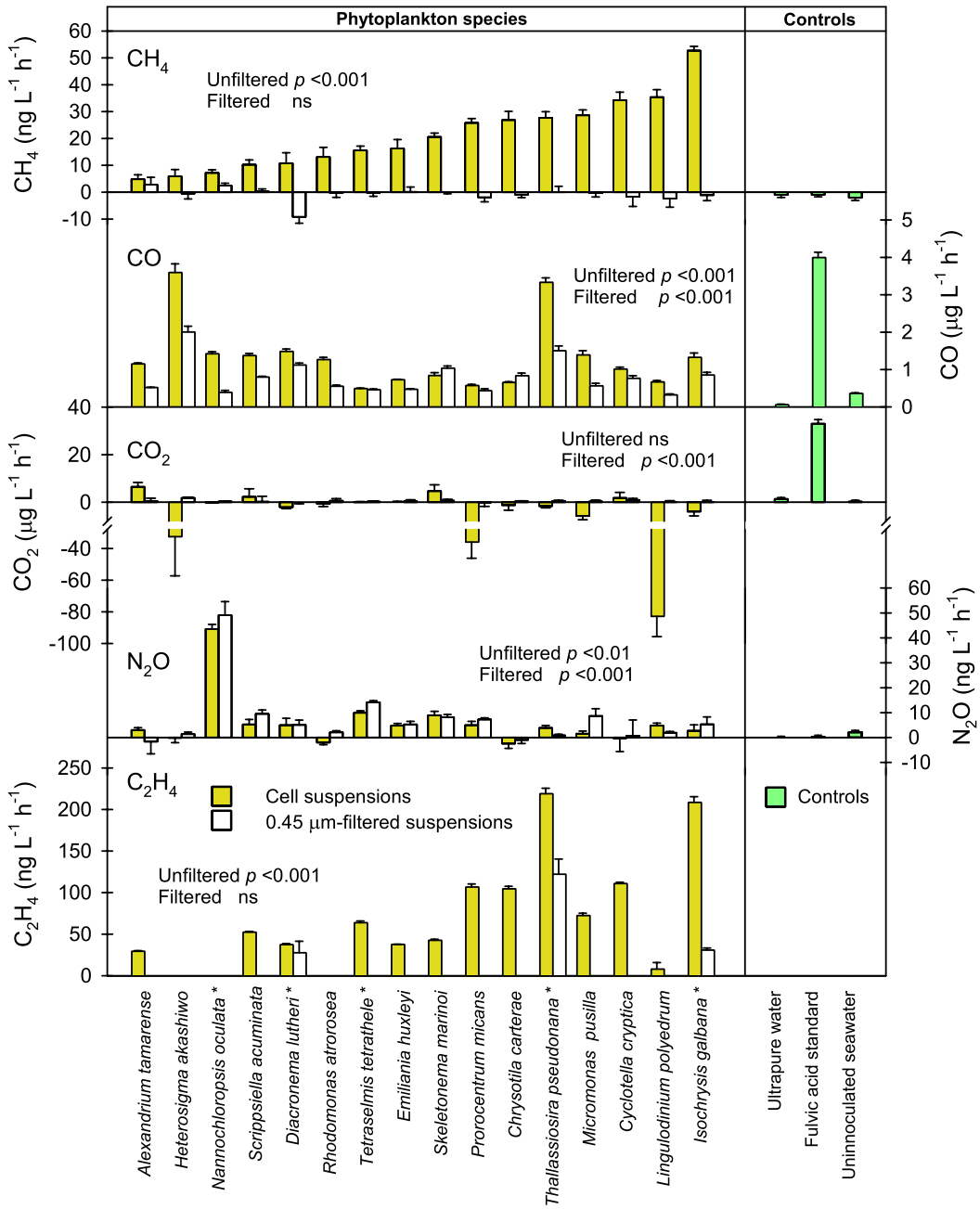

Figure 1. Net UV-induced gas production from 16 species of marine phytoplankton cultured in artificial seawater, without filtration (filled bars) and with 0.45 μm filtration (clear bars), after 8-h irradiation with 8.3 W m^{-2} unweighted UV radiation (280–400 nm) and 1.82 W m^{-2} photosynthetically active radiation (PAR) from Q-Panel UV313 lamps filtered with 125 μm cellulose diacetate at 20°C. * indicates an axenic culture. (a) CH_4; (b) CO; (c) CO_2; (d) N_2O; (e) C_2H_4. Note the variable scales for gas production. Positive values represent emissions, and negative values represent uptake. There was no detectable production of C_2H_6. Vertical bars (where visible) represent mean values ± 1 standard error with $n = 3$ for phytoplankton species and combined data from all experiments for the fulvic acid (NAFA) standard and un-inoculated seawater (with $n = 24$) and ultrapure water (with $n = 16$). Probability values (p) indicate a significant difference or not significant (ns) between pooled values of filtered or unfiltered cell suspensions from all species when tested by the Wilcoxon (Matched Pairs) Signed Rank test ($n = 16$).

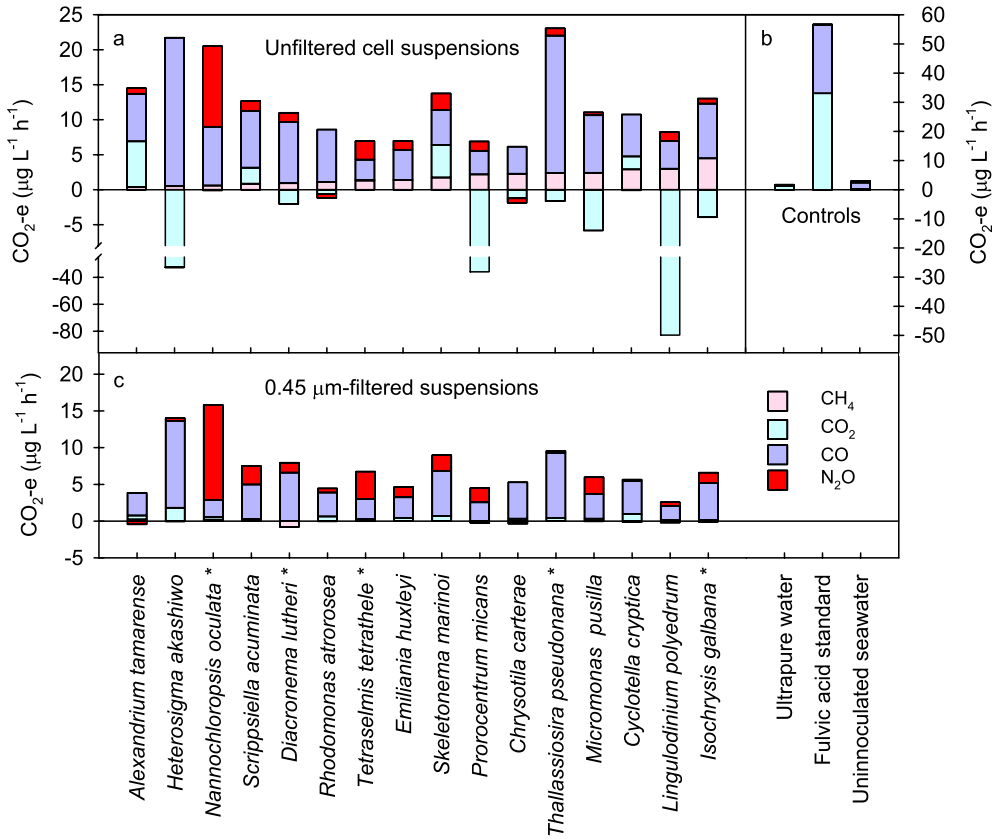

Figure 2. Net UV-induced emissions weighted with the 20-year global warming potential (GWP_{20}) for each gas to give CO_2-equivalent (according to Myhre et al., 2013) after 8-h irradiation with 8.3 W m^{-2} unweighted UV radiation (280–400 nm) and 1.82 W m^{-2} photosynthetically active radiation (PAR) from: (a) cell suspensions of 16 species of marine phytoplankton cultured in artificial seawater; (b) controls: ultrapure water, fulvic acid (NAFA) standard and uninoculated seawater; (c) cell suspensions after 0.45 μm-filtration. * indicates an axenic culture. Positive values represent emissions, negative values represent uptake. Note the break and different scales of *y*-axis.

The overall 20-year CO_2-equivalent (CO_2-e) calculated from the global warming potential (GWP_{20}) for each gas (Myhre et al., 2013) is shown in Figure 2 for each species and controls. Alternative calculations using GWP values for a 100-year time horizon and including a value for C_2H_4 (Forster et al., 2007) are shown in Figures S1 and S2. Spearman rank correlation coefficients (r_s) between each gas produced from cell suspensions and their filtrates are shown in Table 3. Trends in the data for significant correlations ($p < 0.05$) are plotted in Figure S3. Linear regressions were not calculated as only CH_4 emissions from cell suspensions were normally distributed. Significant correlation was only found between CH_4 and C_2H_4 ($r_s = 0.67$, $p < 0.01$) from cell suspensions. Significant positive correlations were detected between CO production from cell suspensions and their filtrates ($r_s = 0.58$, $p < 0.05$) and between N_2O production from cell suspensions and their filtrates ($r_s = 0.72$, $p < 0.05$). However, a negative coefficient was measured between CH_4 production from cell suspensions and filtrates ($r_s = -0.54$, $p < 0.05$) with a clear trend visible (Figure S1c).

3.2. Dissolved and Particulate Carbon and Nitrogen

Values of POC, PON, DOC, and TDN are given in Figure 3 for unfiltered and 0.45 μm-filtered cell suspensions before irradiation and correlation coefficients between these parameters and net gaseous emissions from unfiltered and filtered cell suspensions are shown in Table 3. Significant correlations ($p < 0.05$) were only found between net CO emission from filtered suspensions and their DOC content but there was no visual trend (data not shown).

Table 3
Spearman Rank Correlation Coefficients Between Net Gas Production From 16 Phytoplankton Species and Their Initial Carbon and Nitrogen Content

		Unfiltered cell suspensions					0.45 μm-filtered cell suspensions				
		CH_4	CO_2	CO	N_2O	C_2H_4	CH_4	CO_2	CO	N_2O	C_2H_4
Unfiltered cell suspensions	CH_4	–	−0.40	−0.30	−0.29	**0.67****	**−0.54***	−0.22	−0.02	−0.10	0.29
	CO_2	–	–	−0.14	0.23	−0.04	**0.68****	0.43	0.01	0.04	−0.26
	CO	–	–	–	−0.10	−0.21	0.16	0.17	**0.58***	−0.03	0.47
	N_2O	–	–	–	–	−0.14	0.30	−0.44	−0.32	**0.72****	−0.02
	C_2H_4	–	–	–	–	–	−0.22	−0.23	0.25	−0.07	0.44
0.45 μm-filtered cell suspensions	CH_4	–	–	–	–	–	–	0.36	−0.11	0.21	−0.21
	CO_2	–	–	–	–	–	–	–	0.32	−0.43	−0.33
	CO	–	–	–	–	–	–	–	–	−0.31	**0.54***
	N_2O	–	–	–	–	–	–	–	–	–	−0.14
	C_2H_4	–	–	–	–	–	–	–	–	–	–
POC		0.36	−0.26	0.41	0.13	0.15	−0.32	0.04	0.21	0.05	0.29
PON		0.32	−0.19	0.47	0.20	0.13	−0.26	0.16	0.26	0.24	0.29
DOC		0.27	−0.26	0.41	−0.38	0.37	−0.33	0.32	**0.62***	−0.18	0.41
TDN		−0.16	0.26	−0.07	0.58	−0.01	0.44	−0.09	−0.30	0.05	0.06

Note. POC, particulate organic carbon; PON, particulate organic nitrogen; DOC, dissolved organic carbon; TDN, total dissolved nitrogen. Significant correlations are marked in bold: *, $p < 0.05$; **, $p < 0.01$).

3.3. Actinometry and Photon Fluence Rate

Linear regression was used to estimate the slope of A_{510} of the irradiated ferrioxalate solution to obtain a rate of 0.15 min^{-1}, equivalent to production of 2.04 μmol Fe^{2+} min^{-1} according to Aphalo et al. (2012). Incident radiation was partitioned into total UV and two PAR fractions (corresponding to two far-blue peak emissions at 400–405 and 430–438 nm). The product of quantum yield and fractional absorbance was then used to attribute the Fe^{2+} to each waveband after correction for a calculated mean path length of 1.49 cm (Equation 2),

$$L = \pi \times \frac{r}{2}, \tag{2}$$

where L = mean path length and r = vial internal radius

The photon flux was then applied to the cross sectional area of sample volume to estimate photon fluence for each waveband (Table 4) giving a total of 26.9 μmol m^{-2} s^{-1} over 280–400 nm.

4. Discussion and Conclusions

4.1. UV Exposure

A constant irradiance from an artificial source, rather than ambient sunlight, was selected to allow detection of changes in headspace concentrations over 8-h with minimal depletion of O_2. Our constant irradiance of 4.3 and 4.0 W m^{-2} UVA and UVB provided 8-h integrated doses of 124.1 and 114.9 kJ m^{-2} UVA and UVB, respectively. These compare with global values for monthly mean daily doses calculated using the Tropospheric Ultraviolet-Visible (TUV) model using the mean O_3 column and cloud cover over 11 years (Lee-Taylor & Madronich, 2007) of up to 2,000 kJ m^{-2} day^{-1} UV-A and 60 kJ m^{-2} day^{-1} UV-B. However, it is essential to consider the spectral distribution of artificial sources in order to evaluate their relevance to ambient sunlight due to the differences in UV absorption by different chromophores and the magnitude of effects at different wavelengths (Micheletti et al., 2003). The 0.9:1 ratio of UVB:UVA in this study is higher than in solar radiation where UVB contributes <1% of UV energy. Consequently, experimental observations should not be related to sunlight effects without use of spectral weighting functions for each process (Neale, 2005).

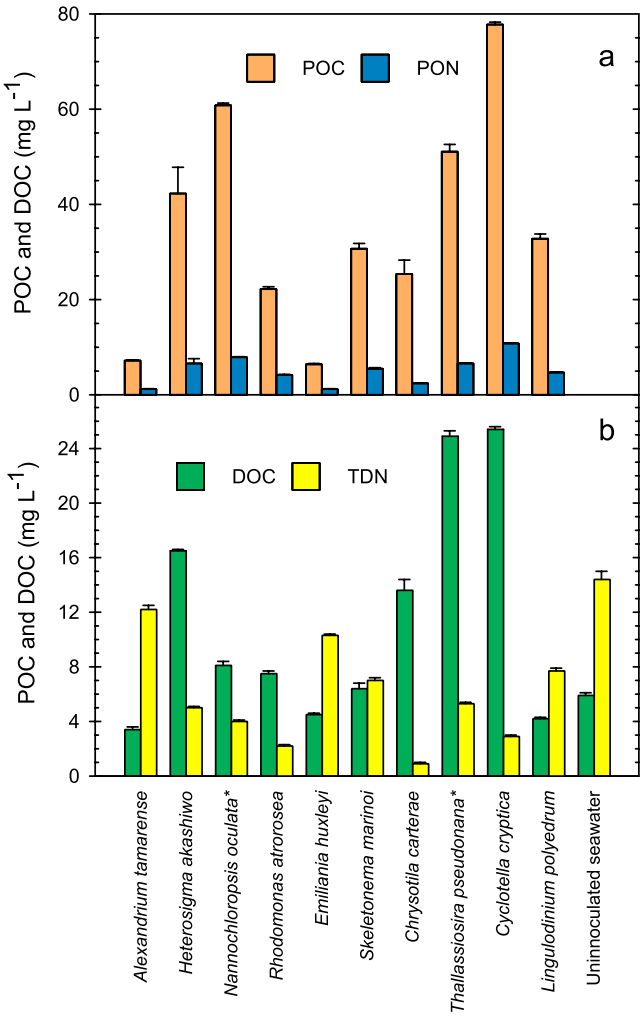

Figure 3. Carbon and nitrogen content of cell suspensions of 10 phytoplankton species and uninoculated seawater before exposure: (a) particulate organic carbon and nitrogen (POC and PON); (b) dissolved organic carbon (DOC) and total dissolved nitrogen (TDN). * indicates an axenic culture. Values are means of two replicates ($n = 2$) ± 1 standard error (s.e.).

In addition, exposure of non-acclimated plants to UVB can induce gene expression via non-specific stress related metabolic pathways (O'Hara et al., 2019) that may not represent effects under sunlight. The experimental exposure was quantified using eight commonly used spectral weighting functions (Table 2) including those for ROS formation and CH_4 emissions from plant pectins. The experimental irradiance weighted for CH_4 production from plant pectin of 5.1 W m^{-2} is lower than the highest values of modeled, similarly weighted, low-latitude irradiance that can exceed 11 W m^{-2} on the CH_4-weighted scale (McLeod et al., 2008).

The planar UV photon irradiance measured by broad band sensor (Table 2) and calibrated by spectroradiometer was 18% lower than the multidirectional UV photon fluence rate of 26.9 µmol m^{-2} s^{-1} measured inside vials by ferrioxalate actinometry (Table 4). One would expect irradiance to be lower because fluorescent lamps provide a multidirectional source geometry that is not perpendicular to the plane of an irradiance sensor. Consequently, the fluence rate provides a theoretically more appropriate estimate of the photons entering the experimental vials.

While the 8-h exposure clearly demonstrated UV-driven emissions, it provided no indication of the relationship between exposure duration and emissions, which are unlikely to be linear if target molecules become significantly depleted. Many exposure response curves are known to be non-linear (Neale, 2005). Additionally, it did not establish reciprocity: the interchangeability between duration and exposure intensity to provide the same dose. In our experiments, cells experienced constant irradiance, whereas the turbulence of the ocean surface mixed layer will reduce exposure as cells move vertically within the water column. UV and PAR are modified with depth in a wavelength dependent manner by the optical properties of the water which are determined by the attenuation of water molecules themselves, chromophoric DOM, phytoplankton cells, and other suspended particulate matter. UV penetration in seawater is therefore greater in open oceans than in coastal areas with UVB attenuation more rapid than UVA and always at least twice that of PAR (UMIRG, 1996). Consequently, exposure to UV at greater depths will be reduced and spectral wavelengths modified. Zaneveld (1975) measured a 10% reduction in UVB by 15 m depth in the open ocean and by 1 m in coastal waters, while Gieskes and Kraay (1990) reported that 10% and more of the UVB measured at the water surface penetrated to 30m in clear Antarctic waters. Lee et al. (2013) reviewed UV-visible attenuation in global oceans and reported that 10% UVA (at 350 nm) was still present at 50–70m depth in oligotrophic waters and clear Antarctic waters. The attenuation of UV with depth is particularly relevant to mixed surface layers of the ocean subject to diurnal stratification, which may extend to 10–50 m depth, in contrast to the typical stratification depth in freshwater systems of ~5 m (Obernos-

Table 4
Photon Fluence Rate Inside Quartz Vials Calculated by Ferrioxalate Actinometry

Wavelength (nm)	Photon irradiance[a] (µmol m^{-2} s^{-1})	Quantum yield (QY)[b]	Fraction absorbed[b]	Fractional partitioning of Fe^{2+} formation	Photonfluence rate (µmol m^{-2} s^{-1})
280–400	22.09	1.26	1.00	0.90	26.9
400–405	0.92	1.16	0.98	0.03	1.1
430–438	3.19	1.11	0.63	0.07	2.5

[a]Photon irradiance as measured by spectroradiometer (see Table 2). [b]Values of QY and fraction absorbed according to Aphalo et al. (2012) with fraction absorbed adjusted for a mean path length of 1.49 cm.

terer et al., 2001). Dose-response relationships covering irradiances below those used in our experiments are therefore necessary in order to integrate natural emissions over depth but these should also take into account the associated spectral changes. Although characterization of UV attenuation is essential, particularly where phytoplankton density is greatest at depth under stratified conditions, many typical conditions in temperate latitudes with storm-induced turbulence have a well-mixed surface layer and more uniform distribution of phytoplankton. Under these conditions, turbulent mixing will replenish the upper photic zone subject to highest UV irradiance with cells and particulates from below with less-depleted substrate molecules for photochemical action. Smith and Baker (1979) observed that phytoplankton do make a significant contribution to UV attenuation in the open oceans where DOM concentrations are low. Individual organisms may also modify their adaptive responses to UV by changes in physiology, biochemistry and behavior including the production of both intracellular and extracellular UV protective pigments (Roy, 2005).

Photochemical production rates are ideally related to photon absorption and temperature using spectrally dependent apparent quantum yields, which are essential for accurate estimation of global production of trace gases (Mopper et al., 2015). Consequently, our study illustrates the potential of UV to drive gaseous emissions from phytoplankton cells, and appropriate quantification of ambient UV effects requires detailed dose-response studies at appropriate wavelengths.

Short wavelength PAR should also be considered in photochemical gas production because blue light has photochemical effects in several environments: influencing marine DOM degradation through generation of reactive radicals including OH (Mopper & Kieber, 2005); causing 468 nm photochemical damage to retinal cells by ROS generation in human eyes (Ozkaya et al., 2019); and in photodegradation of terrestrial leaf litter not only in semi-arid environments (Austin & Vivanco, 2006; Austin et al., 2016) but also on the forest floor (Pieristè et al., 2019; Wang et al., 2020). Lee et al. (2013) observed that blue-green wavelengths of PAR penetrate ~30%–40% deeper than the commonly used depth of the euphotic zone in oceanic waters. The recent observations that ^{13}C label in cultured phytoplankton can be observed in CH_4 emissions and increases with higher irradiance (Hartmann et al., 2020; Klintzsch et al., 2019, 2020) warrants further investigation to assess short wavelength PAR photochemistry of cells and their exudates, because experimental light sources can produce significant violet and blue wavelengths, which can include a broad 450 nm peak (e.g., Klintzsch et al., 2020).

4.2. Methane Production

UV exposure of cells of most species produced net CH_4 ranging between 4.8 and 53 ng CH_4 L^{-1} h^{-1}, with only two species producing detectable CH_4 from the filtered suspension (Figure 1a), indicating that photochemical transformation of cell structural components, metabolism, or DOM released during irradiation may produce emissions rather than DOM released during prior growth. No net CH_4 production was detected from the NAFA standard, un-inoculated seawater, or ultrapure water. A negative correlation coefficient and linear trend were observed between CH_4 production from cell suspensions and their filtrates (Figure S1c). There is potential for methanotrophy in bacteria associated with non-axenic phytoplankton cultures, with possible activity related to their host potential to generate CH_4, so that bacterial cells in filtrates might explain this relationship. However, the filtrate from the axenic *I. galbana* had the highest decrease in headspace CH_4 on irradiation which does not support this hypothesis, and suggests bacterial presence should be directly tested in future experiments.

Li et al. (2020) used a solar simulator to measure the CH_4:CO photoproduction ratio of CDOM in 0.2 μm-filtered water samples and its relationship with the 320 nm absorption coefficient to estimate global open-ocean CH_4 photoproduction of ~0.12 Tg $year^{-1}$ and acknowledged that this may be 20%–40% higher if POM is also considered. Their CH_4 photoproduction rates of $\sim 1 \times 10^{-3}$ nmol L^{-1} h^{-1} from open-ocean CDOM are greatly exceeded by our rates from irradiated cell suspensions of 0.3–3.3 nmol L^{-1} h^{-1} (Table S1).

Lenhart et al. (2016) measured CH_4 emission from *E. huxleyi* cultures grown under visible light and demonstrated incorporation of ^{13}C-label into CH_4 from labeled HCO_3^- and the methyl thioether group of methionine in the growth medium. Oxic CH_4 production by *E. huxleyi* cultures, grown under visible light, was also demonstrated by Klintzsch et al. (2019), who showed that ^{13}C-label in three methylated sulfur compounds: DMSO, DMS, and methionine sulphoxide was incorporated into CH_4. Their production rates

of 0.7 and 3.1 μg CH_4 g^{-1} POC d^{-1}, respectively, from cultures in an exponential growth phase, are much lower than our rate of 2.56 μg CH_4 g^{-1} POC h^{-1} due to our higher measured POC values. Subsequently, Klintzsch et al. (2020) showed that the level of PAR could control CH_4 production by over an order of magnitude and was increased by continuous illumination compared to a 6/18h light cycle. Microbial degradation of DOM phosphonates was shown to produce CH_4 and C_2H_4 by Repeta et al. (2016), Perez-Coronel and Beman (2020), and Sosa et al. (2020), while Bižić et al. (2020) reported CH_4 production from metabolism of 17 marine, freshwater, and terrestrial cyanobacteria (independent of methylated precursors e.g., methylphosphonate). Bižić et al. (2020) measured rates of 1.6–54.6 μg CH_4 g^{-1} dry weight (DWT) h^{-1} from cyanobacteria under a light/dark cycle of visible light (but no UV) and under dark, oxic, and anoxic conditions, suggesting that cyanobacteria could make important contributions to oceanic CH_4 supersaturation. Their emission rates from cyanobacteria were higher than published rates from eukaryotic plants and *E. huxleyi*. Although they reported dark CH_4 production in cyanobacteria, we observed no statistical significance ($p = 0.6$) for dark CH_4 production from our pooled data for 16 eukaryote species (Table S2) despite our method detecting UV-driven CH_4 production of similar magnitude to other studies (e.g., Klintzsch et al., 2019; Lenhart et al., 2016). Most recently, Hartmann et al. (2020) demonstrated CH_4 production by cyanobacteria, diatoms, chlorophytes and cryptophytes from the freshwater Lake Stechlin and *in situ* production using floating chambers.

4.3. Carbon Monoxide Production

Carbon monoxide is supersaturated in surface oceans with respect to the atmosphere and photochemical production is the major source (Reader & Miller, 2012). UV-driven CO production was observed from cell suspensions of all species (Figure 1b), but in contrast to CH_4, CO was also produced during UV exposure of all filtrates, although at lower rates than from the unfiltered cell suspensions. This suggests that DOM released during growth before exposure was also a source of CO and is reflected in the correlation ($r_s = 0.58$, $p < 0.05$) between CO production from cell suspensions and their filtrates (Table 3). Mopper et al. (1991) measured sunlight-driven CO production from Sargasso Sea waters of 1–20 m depth as 18.6 nmol L^{-1} C h^{-1} which is significantly higher than any measured CO production in our experiments that ranged from 0.02 to 0.13 nmol L^{-1} h^{-1} (Table S1).

Irradiation of the NAFA standard, which contains a variable structure including carboxylic and phenolic functional groups (Nada et al., 2019), produced more CO (and CO_2) than all other samples. CO (and small amounts of CO_2) production from un-inoculated seawater most likely originated from the Ultramarine Sea Salt, which contains unlisted trace amounts of fish vitamins (M. Sullivan, Waterlife Research Industries, Longford, UK, personal communication, February 5, 2018), and production from ultrapure water likely originated from DOC released from the exchange reagent used in de-ionisation.

4.4. Carbon Dioxide Production

Headspace concentration changes revealed production or uptake of CO_2 but do not account for changes in the $CO_2/HCO_3/CO_3$ equilibrium resulting from uptake of aqueous CO_2 or HCO_3^- during photosynthesis. Measurement of salinity and changes in any two parameters from pH, alkalinity, or dissolved inorganic C during irradiation would enable calculation of equilibrium values using a variety of available computing packages (Orr et al., 2015), but they were not measured in our experiment. Photochemical processes and cell respiration by phytoplankton and bacteria can generate CO_2, and it has been suggested that UV exposure can increase dark respiration in higher plants due to enhanced protection and repair metabolism (Gwynn-Jones, 2001). Beardall et al. (1997) observed both increased and decreased respiration immediately after UV and PAR irradiation in two freshwater algal species. Vernet (2005) concluded there was no evidence for increasing phytoplankton respiration after UV exposure and that respiration should be measured during both exposure and acclimation because repair processes could affect respiration rates. Increased respiratory CO_2 emissions would add to any photochemical production during our experiments. UV-induced cell death leading to a loss of respiratory CO_2 output is also a possibility but any cell lysis could also release DOM and enhance photochemical or microbial production of CO_2 and other gases. Four species did show a net reduction of headspace CO_2 after UV exposure (Figure 1c) suggesting photosynthetic uptake, but there was no clear relationship with other gas production and no correlation between CO_2 and other gases in unfil-

tered samples (Table 3). Some species of phytoplankton and benthic marine algae have light compensation points below 2 μmol m^{-2} s^{-1} PAR (Richardson et al., 1983), so, net photosynthesis may have occurred at the 7.2 μmol m^{-2} s^{-1} PAR in our experiments, while some higher plants and marine macroalgae can use UVA wavelengths to drive photosynthesis (Turnbull et al., 2013; Xu & Gao, 2016). Booth et al. (1997) reported a threshold for photosynthetic inhibition in Antarctic phytoplankton of 0.5 W m^{-2} UVB and 10 W m^{-2} UVA. This UVB value was exceeded in our experiments and may indicate possible UV tolerance in *H. akashiwo*, *M. pusilla*, *P. micans*, and *L. polyedrum*.

The total CO_2-e over a 20-year time horizon from other gases (Figure 2) was more than compensated by the CO_2 uptake in three species at the level of PAR used in our experiments. Photosynthetic uptake of CO_2 may have occurred in other species but compensated by photochemical CO_2 production from components of the cell structure or exudates during growth before or during irradiation. Values of GWP were chosen rather than the sustained-flux GWP (SGWP; Neubauer, 2021) because our experiments represent a pulse emission of short duration. Over a longer time horizon of 100 years, the GWP value for CH_4 and CO decreases from 85 to 30 and from 5.9 to 1.9, respectively, (Neubauer, 2021), illustrating their decreased significance to experimental CO_2-e at longer time scales (Figure S1). Figure S2 also shows CO_2-e using earlier estimates of GWP (Forster et al., 2007) that also include C_2H_4, illustrating the relatively small contribution from this gas.

The mole ratio of CO_2:CO photoproduction from marine DOM is reported to range between ~2 and 98 (White et al., 2010) and to vary with the DOM source and content (Reader & Miller, 2012). However, Erickson et al. (2015) report that an average ratio for oceanic marine samples is ~20 but somewhat lower in freshwaters. The ratio of CO_2:CO production was most likely modified during our experiments by photosynthetic uptake of CO_2 and/or release of DOM during exposures, but the ratios of emissions from filtrates (calculated from Table S1) were very low with the highest value of 0.8 from *C. cryptica* filtrate, whereas the value from the NAFA standard was 5.3. Although 0.45 μm filtration removes phytoplankton cells of all 16 species studied, bacterial presence in the cell suspensions and filtrates could be an important factor influencing the CO_2:CO ratio in non-axenic species via uptake and metabolism of cell exudates. However, filtrates from all five axenic cultures had even lower ratios, suggesting that culture exudates may not produce a high proportion of CO_2 under the wavelengths of our UV irradiation. The observation of positive CO_2 production from cells >0.45 μm (irradiated unfiltered suspensions minus irradiated filtered suspensions, see Table S2) indicates a possible source from cell structural components, from organic exudates or from enhanced respiration of phytoplankton cells (or any bacterial associates) during exposure. Vachon et al. (2016) suggest that UV in a solar simulator most likely inactivated any bacteria during their experiments. However, further studies filtering suspensions with a 0.1–0.2 μm pore size to remove microbial cells would be useful to examine the role of bacterial associates in studies of cultured or natural phytoplankton populations.

4.5. Nitrous Oxide Production

The water column of all major ocean basins, most marginal seas, and numerous estuaries contains dissolved N_2O (Bange et al., 2019) and while the oceans are a major natural contributor to atmospheric N_2O, quantitative estimates remain highly uncertain (Buitenhuis et al., 2018). It is generally thought to be generated as a by-product of nitrification and an intermediate in denitrification (Bange, 2006). We are not aware of any estimates of photochemical N_2O formation from marine phytoplankton, but photochemical production of nitric oxide (NO) and nitrogen dioxide (NO_2) from marine DOM (Mopper & Kieber, 2005) and breakdown of humic material is considered a source of nitrogen for phytoplankton (Kieber, 2005). However, UV photoproduction of N_2O from higher plants was reported by Bruhn et al. (2014). Lenhart et al. (2015) measured non-photochemical production of N_2O from a range of terrestrial cryptogamic communities of cyanobacteria, algae, fungi, lichens, and bryophytes, ranging from 0.5 to 26.3 ng g^{-1} DWT h^{-1} and from a range of higher plant species with a mean of 13.4 ng N_2O g^{-1} DWT h^{-1} under sterile conditions and 30.4 ng N_2O g^{-1} DWT h^{-1} under non-sterile conditions (Lenhart et al., 2019). Our highest N_2O production from irradiation of the axenic *N. oculata* (Figure 1d) was similar to rates from filtrates and consequently production appears to result from cell exudates prior to irradiation. This is also supported by a correlation ($r_s = 0.72$, $p < 0.01$) between N_2O emission from unfiltered cell suspensions and their filtrates (Table 3). Lenhart et al. (2015) scaled their estimates of emissions from cryptogamic covers to estimate global production as a ratio with respiratory CO_2 and found it accounted for 4%–9% of the natural terrestrial N_2O emissions of ~0.45 Tg yr^{-1}.

Consequently, any cell exudates contributing to N_2O emissions, particularly from phytoplankton blooms, warrant further investigation in natural sunlight as they may constitute a local or regional N_2O source.

4.6. Ethene Production

Several studies have found ocean surface C_2H_4 concentrations in excess of atmospheric equilibrium (Seifert et al., 1999). It can be produced by microalgae and seaweeds and Sosa et al. (2020) recently demonstrated C_2H_4 (and CH_4) production from microbial metabolism of organic phosphorus compounds in oligotrophic ocean regions. However, photochemical breakdown of DOC has been suggested as the main oceanic source and demonstrated using PAR in several studies (Plettner et al., 2005). C_2H_4 is a well-researched higher plant hormone with multiple roles that mediate adaptive responses during growth and in response to stress conditions, including high light intensity, which Plettner et al. (2005) suggest may also be relevant in aquatic environments. They summarized published rates of C_2H_4 emission from microalgae and higher plants including their own study of the marine macroalga *Ulva intestinalis* L., which produced between 0.02 and 0.9 ng C_2H_4 g^{-1} DWT h^{-1} under 120 μmol m^{-2} s^{-1} PAR. Sawada and Totsuka (1986) approximated C_2H_4 production to 4.1 ng g^{-1} DWT h^{-1} based on 30 data sources for grasses, herbs and trees in order to estimate global emissions. Fraser et al. (2015) reported rates for 30 species of higher plant foliage under irradiation of 11.6 W m^{-2} unweighted UV when 29 species showed net C_2H_4 emission between 4.7 and 131 ng g^{-1} DWT h^{-1}. Our rates from UV irradiation of phytoplankton (using the same type of lamp source) between 0 and 6 μg C_2H_4 g^{-1} POC h^{-1} (Figure 1e) were much higher than the rates noted above for marine macroalgae and phytoplankton under PAR. Fraser et al. (2015) observed a significant correlation between C_2H_4 and CH_4 emissions which we also observed in our data (Figure S3) supporting the possibility that these emissions are a metabolic UV stress response rather than photochemistry at cell surfaces. Although C_2H_4 contributed a small fraction of CO_2-e emissions (Figure S2) this suggests that C_2H_4 emissions from phytoplankton blooms warrant further investigation in sunlight, particularly as blooms are increasing (Richardson et al., 2019; Riebesell et al., 2018) and the potential for C_2H_4 to act as an infomolecule within and between phytoplankton cells (Plettner et al., 2005).

4.7. Cell Structure, Density, and Excretion of DOM

Variable growth rates, physiological condition, and cell densities between cultures may all cause variation in gas production that cannot be conclusively attributed to species differences. However, there is considerable diversity between species in cell structure, contents and exudates, their potential chromophores and substrates for photochemical breakdown. Some are "naked" (i.e., lacking rigid cell walls e.g., the chlorophyte *M. pusilla* and the ochrophyte *H. akashiwo*), some have scales (e.g., the chlorophyte *T. tetrathele)* or cellulose-containing thecal plates covering the cell surface (e.g., the dinoflagellate *Alexandrium* spp. [Touzet et al., 2010]), others have calcified platelets (e.g., the coccolith *E. huxleyi* [Borowitzka, 2018]) or siliceous frustules (e.g., the diatom *T. pseudonana* (Tomas, 1997)), while others can produce large quantities of extracellular polysaccharides surrounding cells (e.g., the prymnesiophyte *Phaeocystis* spp). Other species release UV-absorbing compounds into the surrounding water and can contain intracellular protective pigments (Roy, 2005; Vernet & Whitehead, 1996). Some diatoms and dinoflagellates form blooms with an accumulation of gelatinous masses at and below the surface (e.g., covering >10,000 km^2 in the Adriatic Sea during summer months (Myklestad, 1995)). Most phytoplankton species exhibit both passive and active DOM exudation during all phases of growth, including from healthy cells. The DOM quality may vary with nutrient limitations (Pete et al., 2010) and is often a constant proportion of total photosynthetic rate, which Vernet (2005) suggests comprises 5%–25% of carbon incorporated into particulate matter in both monocultures and natural populations. Exudates vary between species but generally comprise ~80% carbohydrates plus amino acids, proteins, nucleic acids and lipids (Carlson & Hansell, 2015), often increasing at higher light intensity and under stress conditions (Carlson & Hansell, 2015; Myklestad, 1995; Vernet, 2005). These exudates are likely to contain chromophoric components that absorb UV or visible radiation and may facilitate indirect photochemistry of non-absorbing molecules to generate gas emissions, which was demonstrated for several non-absorbing carbohydrates by addition of the photosensitizer tryptophan (Messenger et al., 2009).

Direct UV effects could also modify the amount or type of DOC release, or cause cell lysis during long irradiations, which could then undergo photochemical transformation or increase heterotrophic microbial activity. Future experiments would ideally monitor cell numbers and biomass and measure changes in the amount and type of DOC before and after irradiation. It would also be useful to measure Fe speciation and availability, which exerts a control on phytoplankton productivity in up to half of the world's oceans (Moore et al., 2001), as DOC can strongly complex and bind Fe (Laglera & van den Berg, 2009) and there is a potential for ROS generation from catalytic reactions between Fe-containing nanoparticles and DOC in the photic zone of aquatic systems (Huang et al., 2020).

While our results demonstrate UV-driven gas production from cell suspensions, these are at higher cell densities than found in most of the open ocean. However, dense algal blooms covering large areas do approach these experimental densities, for example, a bloom of *E. huxleyi* in the North-east Atlantic Ocean covered ~250,000 km^2 and was visible from space (Holligan et al., 1993). Vernet et al. (1989) reported 9.4×10^6 cells L^{-1} comprising 99% *P. micans* in red tide populations off La Jolla, CA, USA. Smith et al. (1992) observed $1–4 \times 10^6$ cells L^{-1} of a *Phaeocystis* sp. in the marginal ice zone of the Southern Ocean experiencing increased UVB from stratospheric O_3 depletion and Tyrrell and Merico (2004) reported blooms of *E. huxleyi* up to 10×10^6 L^{-1} at some locations globally. These densities are higher or similar to those used in our experiments and phytoplankton blooms are expected to show changes in frequency, size, distribution and types of organism with global change effects on climate, eutrophication in coastal zones and ocean circulation and stratification (Ralston & Moore, 2020; Townhill et al., 2018).

Our results clearly demonstrate a potential for UV radiation to result in emission of CH_4, N_2O, and C_2H_4 as well as CO and CO_2 from a range of marine phytoplankton cells during growth. This may result from photodegradation of cell components or cell metabolism including a response to UV stress. These gases all make direct or indirect contributions to radiative forcing in the atmosphere or stratospheric ozone chemistry (Bais et al., 2019; IPCC, 2013). However, it remains necessary to investigate the process further in the field using natural sunlight, and to determine and apply appropriate spectral weighting functions to global models of UV and visible radiation, in order to estimate the full significance for future global changes in plankton growth and distribution, ocean surface stratification and UV irradiance. Modelling of UV-driven emissions from aquatic sources requires inclusion of a range of factors including spectral water transparency and depth of the surface mixed layer such as those as used in current models of photochemical fluxes and UV effects on phytoplankton photosynthesis (e.g., Fichot & Miller, 2010; Neale & Thomas, 2017). All components of seston comprising living organic matter (mainly phytoplankton, but including zooplankton) and tripton (non-living organic matter comprising organic detritus and inorganic particles, including buoyant microplastics) may contribute to photochemical emissions. There are many studies that report production of CH_4 and other gases in aquatic systems that are associated with phytoplankton growth, chlorophyll content, biomass, POC and irradiance level, clearly demonstrating links to phytoplankton of several types (Donis et al., 2017; Tang et al., 2016; Ye et al., 2019). There are also recent studies (Bižić et al., 2020; Klintzsch et al., 2019, 2020, 2020; Perez-Coronel & Beman, 2020; Repeta et al., 2016) reporting CH_4 production from phytoplankton metabolism linked to temperature and visible irradiance. However, UV and visible photochemistry of cell structure and exudates may also contribute to emissions of CH_4 and other climate-relevant gases, with more rapid attenuation of UV wavelengths making them more effective at shallower depths. These gases may consequently affect microbial processes at phytoplankton and particle surfaces, in the boundary layer surrounding cells, on components of the surface microfilm at the air/sea interface and at a local or regional scale, especially in the vicinity of concentrated phytoplankton blooms which are predicted to change in prevalence and distribution with future global change scenarios. Many environmental factors influencing these processes will be affected by global changes in the level and distribution of UV and visible irradiation, land use changes in nutrient inputs of terrigenous DOM to the oceans, and changes in ocean circulation which may all modify phytoplankton growth and abundance. It is essential to fully understand the role of UV and visible photochemistry in the field in order to fully evaluate the significance of future global warming, ocean acidification and eutrophication on biogeochemical cycles.

Conflict of Interest

The authors declare no conflicts of interest relevant to this study.

Data Availability Statement

Datasets for this research are available in the institutional repository of the University of Edinburgh (https://doi.org/10.7488/ds/3106).

Acknowledgments
The authors thank Richard Abell, Kirsty Crockett, David Green, Sian Henley, Zoe Popper, Matt Robson, and Keith Smith for helpful discussions, Joanne Field and Cecilia Rad Menéndez for preparation of the algal cultures, and Colin Abernethy and Sharon McNeill for completion of analyses. Numerical values for the biological weighting function for photosynthesis inhibition in marine picophytoplankton were kindly provided by Professor Patrick Neale. Financial support was provided by the Carnegie Trust for the Universities of Scotland (Collaborative Research Award 50214).

References

Althoff, F., Benzing, K., Comba, P., McRoberts, C., Boyd, D. R., Greiner, S., & Keppler, F. (2014). Abiotic methanogenesis from organosulphur compounds under ambient conditions. *Nature Communications*, *5*. https://doi.org/10.1038/ncomms5205

Aphalo, P. J., Albert, A., Bjorn, L. O., McLeod, A., Robson, T. M., & Rosenqvist, E. (Eds.). (2012). *Beyond the visible: A handbook of best practice in plant UV photobiology*. Helsinki: University of Helsinki, Division of Plant Biology: COST Action FA0906 UV4 growth.

Austin, A. T., Mendez, M. S., & Ballare, C. L. (2016). Photodegradation alleviates the lignin bottleneck for carbon turnover in terrestrial ecosystems. *Proceedings of the National Academy of Sciences of the United States of America*, *113*(16), 4392–4397. https://doi.org/10.1073/pnas.1516157113

Austin, A. T., & Vivanco, L. (2006). Plant litter decomposition in a semi-arid ecosystem controlled by photodegradation. *Nature*, *442*(7102), 555–558.

Bais, A. F., Bernhard, G., McKenzie, R. L., Aucamp, P. J., Young, P. J., Ilyas, M., et al. (2019). Ozone-climate interactions and effects on solar ultraviolet radiation. *Photochemical and Photobiological Sciences*, *18*(3), 602–640. https://doi.org/10.1039/c8pp90059k

Bange, H. W. (2006). Nitrous oxide and methane in European coastal waters. *Estuarine, Coastal and Shelf Science*, *70*(3), 361–374. https://doi.org/10.1016/j.ecss.2006.05.042

Bange, H. W., & Uher, G. (2005). Photochemical production of methane in natural waters: Implications for its present and past oceanic source. *Chemosphere*, *58*(2), 177–183. https://doi.org/10.1016/j.chemosphere.2004.06.022

Bange Hermann, W., Arévalo-Martínez, Damian, L., de la, Paz, Mercedes, F., Laura, K., Jan, K., et al. (2019). A harmonized nitrous oxide (N_2O) ocean observation network for the 21st century. *Frontiers in Marine Science*, *6*(157). https://doi.org/10.3389/fmars.2019.00157

Beardall, J., Berman, T., Markager, S., Martinez, R., & Montecino, V. (1997). The effects of ultraviolet radiation on respiration and photosynthesis in two species of microalgae. *Canadian Journal of Fisheries and Aquatic Sciences*, *54*(3), 687–696. https://doi.org/10.1139/cjfas-54-3-687

Bižić, M., Klintzsch, T., Ionescu, D., Hindiyeh, M. Y., Günthel, M., Muro-Pastor, A. M., et al. (2020). Aquatic and terrestrial cyanobacteria produce methane. *Science Advances*, *6*(3). https://doi.org/10.1126/sciadv.aax5343

Booth, C. R., Morrow, J. H., Coohill, T. P., Cullen, J. J., Frederick, J. E., Hader, D. P., et al. (1997). Impacts of solar UVR on aquatic microorganisms. *Photochemistry and Photobiology*, *65*(2), 252–253. https://doi.org/10.1111/j.1751-1097.1997.tb08550.x

Borowitzka, M. A. (2018). Biology of Microalgae. In I. A. Levine & J. Fleurence (Eds.), *Microalgae in health and disease prevention* (pp. 23–72): Academic Press.

Breitbarth, E., Mills, M. M., Friedrichs, G., & LaRoche, J. (2004). The Bunsen gas solubility coefficient of ethylene as a function of temperature and salinity and its importance for nitrogen fixation assays. *Limnology and Oceanography: Methods*, *2*, 282–288.

Bruhn, D., Albert, K. R., Mikkelsen, T. N., & Ambus, P. (2014). UV-induced N_2O emission from plants. *Atmospheric Environment*, *99*, 206–214. https://doi.org/10.1016/j.atmosenv.2014.09.077

Bruhn, D., Moller, I. M., Mikkelsen, T. N., & Ambus, P. (2012). Terrestrial plant methane production and emission. *Physiologia Plantarum*, *144*(3), 201–209. https://doi.org/10.1111/j.1399-3054.2011.01551.x

Buitenhuis, E. T., Suntharalingam, P., & Le Quéré, C. (2018). Constraints on global oceanic emissions of N_2O from observations and models. *Biogeosciences*, *15*(7), 2161–2175. https://doi.org/10.5194/bg-15-2161-2018

Caldwell, M. M. (1971). Solar ultraviolet radiation and the growth and development of higher plants. In A. C. Giese (Ed.), Photophysiology (Vol. 6, pp. 131–177). New York: Academic Press.

Carlson, C. A., & Hansell, D. A. (2015). DOM Sources, Sinks, Reactivity, and Budgets. In D. A. Hansell, & C. A. Carlson (Eds.), *Biogeochemistry of marine dissolved organic matter* (2nd ed., pp. 66–126). London: Academic Press.

Cory, R. M., Ward, C. P., Crump, B. C., & Kling, G. W. (2014). Sunlight controls water column processing of carbon in arctic fresh waters. *Science*, *345*(6199), 925–928. https://doi.org/10.1126/science.1253119

Donis, D., Flury, S., Stöckli, A., Spangenberg, J. E., Vachon, D., & McGinnis, D. F. (2017). Full-scale evaluation of methane production under oxic conditions in a mesotrophic lake. *Nature Communications*, *8*(1), 1661. https://doi.org/10.1038/s41467-017-01648-4

Erickson, D. J., Sulzberger, B., Zepp, R. G., & Austin, A. T. (2015). Effects of stratospheric ozone depletion, solar UV radiation, and climate change on biogeochemical cycling: Interactions and feedbacks. *Photochemical and Photobiological Sciences*, *14*(1), 127–148. https://doi.org/10.1039/c4pp90036g

Fichot, C. G., & Miller, W. L. (2010). An approach to quantify depth-resolved marine photochemical fluxes using remote sensing: Application to carbon monoxide (CO) photoproduction. *Remote Sensing of Environment*, *114*(7), 1363–1377. https://doi.org/10.1016/j.rse.2010.01.019

Flint, S. D., & Caldwell, M. M. (2003). A biological spectral weighting function for ozone depletion research with higher plants. *Physiologia Plantarum*, *117*(1), 137–144.

Forster, P., Ramaswamy, V., Artaxo, P., Berntsen, T., Betts, R., Fahey, D. W., et al. (2007). Changes in atmospheric constituents and in radiative forcing. In Solomon, S., D. Qin, M. Manning, Z. Chen, M. Marquis, K. B. Averyt, M. Tignor & H. L. Miller (Eds.), *Climate change 2007: The physical science basis. Contribution of working group I to the fourth assessment report of the Intergovernmental Panel on climate change* (pp. 129–234). Cambridge: Cambridge University Press

Fraser, W. T., Blei, E., Fry, S. C., Newman, M. F., Reay, D. S., Smith, K. A., & McLeod, A. R. (2015). Emission of methane, carbon monoxide, carbon dioxide and short-chain hydrocarbons from vegetation foliage under ultraviolet irradiation. *Plant, Cell and Environment*, *38*(5), 980–989. https://doi.org/10.1111/pce.12489

Ghetti, F., Herrmann, H., Hader, D. P., & Seidlitz, H. K. (1999). Spectral dependence of the inhibition of photosynthesis under simulated global radiation in the unicellular green alga Dunaliella salina. *Journal of Photochemistry and Photobiology B: Biology*, *48*(2–3), 166–173. https://doi.org/10.1016/s1011-1344(99)00043-3

Gieskes, W. W. C., & Kraay, G. W. (1990). Transmission of ultraviolet light in the Weddell Sea: Report of the first measurements made in the Antarctic. *BIOMASS Newsletter 12*:12–14.

Green, A. E. S., Sawada, T., & Shettle, E. P. (1974). The middle ultraviolet reaching the ground. *Photochemistry and Photobiology*, *19*, 251–259.

Guillard, R. R., & Ryther, J. H. (1962). Studies of marine planktonic diatoms. 1. *Cyclotella nana hustedt,* and *Detonula confervacea* (Cleve) gran. *Canadian Journal of Microbiology*, *8*(2), 229–239.

Günthel, M., Donis, D., Kirillin, G., Ionescu, D., Bizic, M., McGinnis, D. F., et al. (2019). Contribution of oxic methane production to surface methane emission in lakes and its global importance. *Nature Communications*, *10*. https://doi.org/10.1038/s41467-019-13320-0

Günthel, M., Klawonn, I., Woodhouse, J., Bižić, M., Ionescu, D., Ganzert, L., et al. (2020). Photosynthesis-driven methane production in oxic lake water as an important contributor to methane emission. *Limnology & Oceanography*, *65*(12), 2853–2865. https://doi.org/10.1002/lno.11557

Gwynn-Jones, D. (2001). Short-term impacts of enhanced UV-B radiation on photo-assimilate allocation and metabolism: A possible interpretation for time-dependent inhibition of growth. *Plant Ecology*, *154*(1–2), 67–73. https://doi.org/10.1023/a:1012963021074

Hartmann, J. F., Günthel, M., Klintzsch, T., Kirillin, G., Grossart, H.-P., Keppler, F., & Isenbeck-Schröter, M. (2020). High spatiotemporal dynamics of methane production and emission in oxic surface water. *Environmental Science & Technology*, *54*(3), 1451–1463. https://doi.org/10.1021/acs.est.9b03182

Holligan, P. M., Fernandez, E., Aiken, J., Balch, W. M., Boyd, P., Burkill, P. H., et al. (1993). A biogeochemical study of the coccolithophore, *Emiliania huxleyi,* in the North Atlantic. *Global Biogeochemical Cycles*, *7*(4), 879–900. https://doi.org/10.1029/93gb01731

Huang, X., Zhao, Q., Young, R. P., Zhang, X., Walter, E. D., Chen, Y., et al. (2020). Photo-production of reactive oxygen species and degradation of dissolved organic matter by hematite nanoplates functionalized by adsorbed oxalate. *Environmental Science: Nano*, *7*(8), 2278–2292. https://doi.org/10.1039/D0EN00365D

IPCC (2013). *Climate change 2013: The physical science basis. Contribution of working group I to the Fifth Assessment report of the Intergovernmental Panel on Climate Change.* (p. 1535). In: T. F. Stocker, D. Qin, G.-K. Plattner, M. Tignor, S. K. Allen, J. Boschung, A. Nauels, Y. Xia, V. Bex, & P. M. Midgley (Eds.), Cambridge University Press.

Keppler, F., Hamilton, J. T. G., Brass, M., & Röckmann, T. (2006). Methane emissions from terrestrial plants under aerobic conditions. *Nature*, *439*(7073), 187–191.

Kieber, D. J. (2005). Photochemical production of biological substrates. In S. De Mora, S. Demers, & M. Vernet (Eds.), *The effects of UV radiation in the marine environment* (pp. 130–148). Cambridge, UK: Cambridge University Press.

Kieber, D. J., Miller, G. W., Neale, P. J., & Mopper, K. (2014). Wavelength and temperature-dependent apparent quantum yields for photochemical formation of hydrogen peroxide in seawater. *Environmental Science-Processes & Impacts*, *16*(4), 777–791. https://doi.org/10.1039/c4em00036f

Klintzsch, T., Langer, G., Nehrke, G., Wieland, A., Lenhart, K., & Keppler, F. (2019). Methane production by three widespread marine phytoplankton species: Release rates, precursor compounds, and potential relevance for the environment. *Biogeosciences*, *16*(20), 4129–4144. https://doi.org/10.5194/bg-16-4129-2019

Klintzsch, T., Langer, G., Wieland, A., Geisinger, H., Lenhart, K., Nehrke, G., & Keppler, F. (2020). Effects of temperature and light on methane production of widespread marine phytoplankton. *Journal of Geophysical Research: Biogeosciences*, *125*(9), e2020JG005793. https://doi.org/10.1029/2020jg005793

Koehler, B., Landelius, T., Weyhenmeyer, G. A., Machida, N., & Tranvik, L. J. (2014). Sunlight-induced carbon dioxide emissions from inland waters. *Global Biogeochemical Cycles*, *28*(7), 696–711. https://doi.org/10.1002/2014gb004850

Laglera, L. M., & vanden Berg, C. M. G. (2009). Evidence for geochemical control of iron by humic substances in seawater. *Limnology & Oceanography*, *54*(2), 610–619. https://doi.org/10.4319/lo.2009.54.2.0610

Lee, Z. P., Hu, C. M., Shang, S. L., Du, K. P., Lewis, M., Arnone, R., & Brewin, R. (2013). Penetration of UV-visible solar radiation in the global oceans: Insights from ocean color remote sensing. *Journal of Geophysical Research: Oceans*, *118*(9), 4241–4255. https://doi.org/10.1002/jgrc.20308

Lee-Taylor, J., & Madronich, S. (2007). *Climatology of UV-A, UV-B and erythemal radiation at the Earth's surface, 1979-2000*. Boulder: https://doi.org/10.5065/D62J68SZ

Lenhart, K., Behrendt, T., Greiner, S., Steinkamp, J., Well, R., Giesemann, A., & Keppler, F. (2019). Nitrous oxide effluxes from plants as a potentially important source to the atmosphere. *New Phytologist*, *221*(3), 1398–1408. https://doi.org/10.1111/nph.15455

Lenhart, K., Klintzsch, T., Langer, G., Nehrke, G., Bunge, M., Schnell, S., & Keppler, F. (2016). Evidence for methane production by the marine algae *Emiliania huxleyi*. *Biogeosciences*, *13*(10), 3163–3174. https://doi.org/10.5194/bg-13-3163-2016

Lenhart, K., Weber, B., Elbert, W., Steinkamp, J., Clough, T., Crutzen, P., et al. (2015). Nitrous oxide and methane emissions from cryptogamic covers. *Global Change Biology*, *21*(10), 3889–3900. https://doi.org/10.1111/gcb.12995

Li, Y., Fichot, C. G., Geng, L., Scarratt, M. G., & Xie, H. (2020). The contribution of methane photoproduction to the oceanic methane paradox. *Geophysical Research Letters*, *47*(14). https://doi.org/10.1029/2020gl088362

McKay, W. A., Turner, M. F., Jones, B. M. R., & Halliwell, C. M. (1996). Emissions of hydrocarbons from marine phytoplankton - Some results from controlled laboratory experiments. *Atmospheric Environment*, *30*(14), 2583–2593. https://doi.org/10.1016/1352-2310(95)00433-5

McKinlay, A. F., & Diffey, B. L. (1987). A reference action spectrum for ultra-violet induced erythema in human skin. In W. F. Passchier, & B. F. M. Bosnjakovic (Eds.), *Human exposure to ultra-violet radiation: Risks and regulations* (pp. 83–87). Amsterdam: Elsevier.

McLeod, A. R., Fry, S. C., Loake, G. J., Messenger, D. J., Reay, D. S., Smith, K. A., & Yun, B. W. (2008). Ultraviolet radiation drives methane emissions from terrestrial plant pectins. *New Phytologist*, *180*(1), 124–132. https://doi.org/10.1111/j.1469-8137.2008.02571.x

Messenger, D. J., McLeod, A. R., & Fry, S. C. (2009). The role of ultraviolet radiation, photosensitizers, reactive oxygen species and ester groups in mechanisms of methane formation from pectin. *Plant, Cell and Environment*, *32*(1), 1–9. https://doi.org/10.1111/j.1365-3040.2008.01892.x

Micheletti, M. I., Piacentini, R. D., & Madronich, S. (2003). Sensitivity of biologically active UV radiation to stratospheric ozone changes: Effects of action spectrum shape and wavelength range. *Photochemistry and Photobiology*, *78*(5), 456–461. https://doi.org/10.1562/0031-8655(2003)078<0456:sobaur>2.0.co;2

Moore, J. K., Doney, S. C., Glover, D. M., & Fung, I. Y. (2001). Iron cycling and nutrient-limitation patterns in surface waters of the World Ocean. *Deep-Sea Research Part Ii-Topical Studies in Oceanography*, *49*(1–3), 463–507.

Mopper, K., & Kieber, D. J. (2005). Marine photochemistry and its impact on carbon cycling. In S. De MoraS., Demers, & M. Vernet (Eds.), *The effects of UV radiation in the marine environment* (pp. 101–129). Cambridge: Cambridge University Press.

Mopper, K., Kieber, D. J., & Stubbins, A. (2015). Marine photochemistry of organic matter: Processes and impacts. In D. A. Hansell, & C. A. Carlson (Eds.), *Biogeochemistry of marine dissolved organic matter* (2nd ed., pp. 390–450). London: Academic Press.

Mopper, K., Zhou, X. L., Kieber, R. J., Kieber, D. J., Sikorski, R. J., & Jones, R. D. (1991). Photochemical degradation of dissolved organic carbon and its impact on the oceanic carbon cycle. *Nature*, *353*(6339), 60–62. https://doi.org/10.1038/353060a0

Motulsky, H. (1995). *Intuitive biostatistics*. Oxford University Press.
Myhre, G., Shindell, D., Bréon, F.-M., Collins, W., Fuglestvedt, J., Huang, J., et al. (2013). Anthropogenic and Natural Radiative Forcing. In T. F. Stocker, D. Qin, G.-K. Plattner, M. Tignor, S. K. Allen, J. Boschung, et al. (Eds.), *Climate change 2013: The Physical Science Basis. Contribution of working group I to the Fifth Assessment report of the Intergovernmental Panel on climate change*. (pp. 659–740). Cambridge, United Kingdom and New York, NY, USA: Cambridge University Press
Myklestad, S. M. (1995). Release of extracellular products by phytoplankton with special emphasis on polysaccharides. *The Science of the Total Environment*, *165*(1–3), 155–164. https://doi.org/10.1016/0048-9697(95)04549-g
Nada, M., Grassian, V. H. , & Larsen, S. C. (2019). Zeolites and Mesoporous Silica: From Greener Synthesis to Surface Chemistryof Environmental and Biological Interactions. In A. Douhal, & M. Anpo (Eds.), *Chemistry of silica and Zeolite-based materials* (pp. 375–395): Elsevier.
Neale, P. J. (2005). Spectral weighting functions for quantifying effects of UV radiation in marine ecosystems. In S. De Mora, S. Demers, & M. Vernet (Eds.), *The effects of UV radiation in the marine environment* (pp. 72–100). Cambridge: Cambridge University Press.
Neale, P. J., & Thomas, B. C. (2017). Inhibition by ultraviolet and photosynthetically available radiation lowers model estimates of depth-integrated picophytoplankton photosynthesis: Global predictions for Prochlorococcus and Synechococcus. *Global Change Biology*, *23*(1), 293–306. https://doi.org/10.1111/gcb.13356
Neale, R. E., Barnes, P. W., Robson, T. M., Neale, P. J., Williamson, C. E., Zepp, R. G., et al. (2021). Environmental effects of stratospheric ozone depletion, UV radiation, and interactions with climate change: UNEP Environmental Effects Assessment Panel, Update 2020. *Photochemical and Photobiological Sciences*, *20*, 1–67. https://doi.org/10.1007/s43630-020-00001-x
Neubauer, S. C. (2021). Global warming potential is not an ecosystem property. *Ecosystems*. https://doi.org/10.1007/s10021-021-00631-x
Obernosterer, I., Ruardij, P., & Herndl, G. J. (2001). Spatial and diurnal dynamics of dissolved organic matter (DOM) fluorescence and H_2O_2 and the photochemical oxygen demand of surface water DOM across the subtropical Atlantic Ocean. *Limnology & Oceanography*, *46*(3), 632–643. https://doi.org/10.4319/lo.2001.46.3.0632
O'Hara, A., Headland, L. R., Diaz-Ramos, L. A., Morales, L. O., Strid, A., & Jenkins, G. I. (2019). Regulation of Arabidopsis gene expression by low fluence rate UV-B independently of UVR8 and stress signaling. *Photochemical and Photobiological Sciences*, *18*(7), 1675–1684. https://doi.org/10.1039/c9pp00151d
Orr, J. C., Epitalon, J. M., & Gattuso, J. P. (2015). Comparison of ten packages that compute ocean carbonate chemistry. *Biogeosciences*, *12*(5), 1483–1510. https://doi.org/10.5194/bg-12-1483-2015
Ozkaya, E. K., Anderson, G., Dhillon, B., & Bagnaninchi, P. O. (2019). Blue-light induced breakdown of barrier function on human retinal epithelial cells is mediated by PKC-zeta over-activation and oxidative stress. *Experimental Eye Research*, *189*. https://doi.org/10.1016/j.exer.2019.107817
Perez-Coronel, E., & Beman, J. M. (2020). Biogeochemical and omic evidence for multiple paradoxical methane production mechanisms in freshwater lakes. bioRxiv. https://doi.org/10.1101/2020.07.28.225276
Pete, R., Davidson, K., Hart, M. C., Gutierrez, T., & Miller, A. E. J. (2010). Diatom derived dissolved organic matter as a driver of bacterial productivity: The role of nutrient limitation. *Journal of Experimental Marine Biology and Ecology*, *391*(1–2), 20–26. https://doi.org/10.1016/j.jembe.2010.06.002
Pieristè, M., Chauvat, M., Kotilainen, T. K., Jones, A. G., Aubert, M., Robson, T. M., & Forey, E. (2019). Solar UV-A radiation and blue light enhance tree leaf litter decomposition in a temperate forest. *Oecologia*, *191*(1), 191–203. https://doi.org/10.1007/s00442-019-04478-x
Plettner, I., Steinke, M., & Malin, G. (2005). Ethene (ethylene) production in the marine macroalga *Ulva (Enteromorpha) intestinalis* L. (Chlorophyta, Ulvophyceae): Effect of light-stress and co-production with dimethyl sulphide. *Plant, Cell and Environment*, *28*(9), 1136–1145. https://doi.org/10.1111/j.1365-3040.2005.01351.x
Ralston, D. K., & Moore, S. K. (2020). Modeling harmful algal blooms in a changing climate. *Harmful Algae*, *91*. https://doi.org/10.1016/j.hal.2019.101729
Reader, H. E., & Miller, W. L. (2012). Variability of carbon monoxide and carbon dioxide apparent quantum yield spectra in three coastal estuaries of the South Atlantic Bight. *Biogeosciences*, *9*(11), 4279–4294. https://doi.org/10.5194/bg-9-4279-2012
Repeta, D. J., Ferron, S., Sosa, O. A., Johnson, C. G., Repeta, L. D., Acker, M., et al. (2016). Marine methane paradox explained by bacterial degradation of dissolved organic matter. *Nature Geoscience*, *9*(12), 884–887. https://doi.org/10.1038/ngeo2837
Richardson, J., Feuchtmayr, H., Miller, C., Hunter, P. D., Maberly, S. C., & Carvalho, L. (2019). Response of cyanobacteria and phytoplankton abundance to warming, extreme rainfall events and nutrient enrichment. *Global Change Biology*, *25*(10), 3365–3380. https://doi.org/10.1111/gcb.14701
Richardson, K., Beardall, J., & Raven, J. A. (1983). Adaptation of unicellular algae to irradiance - An analysis of strategies. *New Phytologist*, *93*(2), 157–191. https://doi.org/10.1111/j.1469-8137.1983.tb03422.x
Riebesell, U., Aberle-Malzahn, N., Achterberg, E. P., Alguero-Muniz, M., Alvarez-Fernandez, S., Aristegui, J., et al. (2018). Toxic algal bloom induced by ocean acidification disrupts the pelagic food web. *Nature Climate Change*, *8*(12), 1082-+. https://doi.org/10.1038/s41558-018-0344-1
Roy, S. (2005). Stretgies for the minimisation of UV-induced damage. In S. De Mora, S. Demers, & M. Vernet (Eds.), *The effects of UV radiation in the marine environment* (pp. 177–205). Cambridge University Press.
Royer, S.-J., Ferrón, S., Wilson, S. T., & Karl, D. M. (2018). Production of methane and ethylene from plastic in the environment. *PloS One*, *13*(8), e0200574. https://doi.org/10.1371/journal.pone.0200574
Sawada, S., & Totsuka, T. (1986). Natural and anthropogenic sources and fate of atmospheric ethylene. *Atmospheric Environment*, *20*(5), 821–832. https://doi.org/10.1016/0004-6981(86)90266-0
Seifert, R., Delling, N., Richnow, H. H., Kempe, S., Hefter, J., & Michaelis, W. (1999). Ethylene and methane in the upper water column of the subtropical Atlantic. *Biogeochemistry*, *44*(1), 73–91. https://doi.org/10.1007/bf00992999
Setlow, R. B. (1974). The wavelengths in sunlight effective in producing skin cancer: A theoretical analysis. *Proceedings of the National Academy of Sciences USA*, *71*(9), 3363–3366.
Sharp, J. H., Beuregard, A. Y., Burdige, D., Cauwet, G., Curless, S. E., Lauck, R., et al. (2004). A direct instrument comparison for measurement of total dissolved nitrogen in seawater. *Marine Chemistry*, *84*(3–4), 181–193. https://doi.org/10.1016/j.marchem.2003.07.003
Smith, R. C., & Baker, K. S. (1979). Penetration of UV-B and biologically effective dose rates in natural waters. *Photochemistry and Photobioly*, *29*(2), 311–323. https://doi.org/10.1111/j.1751-1097.1979.tb07054.x
Smith, R. C., Prezelin, B. B., Baker, K. S., Bidigare, R. R., Boucher, N. P., Coley, T., et al. (1992). Ozone depletion: Ultraviolet radiation and phytoplankton biology in Antarctic waters. *Science*, *255*(5047), 952–959. https://doi.org/10.1126/science.1546292

Sosa, O. A., Burrell, T. J., Wilson, S. T., Foreman, R. K., Karl, D. M., & Repeta, D. J. (2020). Phosphonate cycling supports methane and ethylene supersaturation in the phosphate-depleted western North Atlantic Ocean. *Limnology & Oceanography*. https://doi.org/10.1002/lno.11463

Stubbins, A., Law, C. S., Uher, G., & Upstill-Goddard, R. C. (2011). Carbon monoxide apparent quantum yields and photoproduction in the Tyne estuary. *Biogeosciences*, *8*(3), 703–713. https://doi.org/10.5194/bg-8-703-2011

Sulzberger, B., Austin, A. T., Cory, R. M., Zepp, R. G., & Paul, N. D. (2019). Solar UV radiation in a changing world: Roles of cryosphere-land-water-atmosphere interfaces in global biogeochemical cycles. *Photochemical and Photobiological Sciences*, *18*(3), 747–774. https://doi.org/10.1039/c8pp90063a

Sulzberger, B., & Durisch-Kaiser, E. (2009). Chemical characterization of dissolved organic matter (DOM): A prerequisite for understanding UV-induced changes of DOM absorption properties and bioavailability. *Aquatic Sciences*, *71*(2), 104–126. https://doi.org/10.1007/s00027-008-8082-5

Tang, K. W., McGinnis, D. F., Ionescu, D., & Grossart, H. P. (2016). Methane production in oxic lake waters potentially increases aquatic methane flux to air. *Environmental Science and Technology Letters*, *3*(6), 227–233. https://doi.org/10.1021/acs.estlett.6b00150

Tomas, C. R. (Ed.) (1997). *Identifying marine phytoplankton*. San Diego: Academic Press.

Touzet, N., Davidson, K., Pete, R., Flanagan, K., McCoy, G. R., Amzil, Z., et al. (2010). Co-occurrence of the West European (Gr.III) and North American (Gr.I) Ribotypes of *Alexandrium tamarense* (Dinophyceae) in Shetland, Scotland. *Protist*, *161*(3), 370–384. https://doi.org/10.1016/j.protis.2009.12.001

Townhill, B. L., Tinker, J., Jones, M., Pitois, S., Creach, V., Simpson, S. D., et al. (2018). Harmful algal blooms and climate change: Exploring future distribution changes. *ICES Journal of Marine Science*, *75*(6), 1882–1893. https://doi.org/10.1093/icesjms/fsy113

Turnbull, T. L., Barlow, A. M., & Adams, M. A. (2013). Photosynthetic benefits of ultraviolet-A to Pimelea ligustrina, a woody shrub of sub-alpine Australia. *Oecologia*, *173*(2), 375–385. https://doi.org/10.1007/s00442-013-2640-9

Tyrrell, T., & Merico, A. (2004). *Emiliania huxleyi*: Bloom observations and the conditions that induce them. In H. R. Thierstein, & J. R. Young (Eds.), *Coccolithophores* (pp. 75–97). Berlin, Heidelberg: Springer.

UMIRG (1996). *The potential impacts of ozone depletion in the United Kingdom. Report of the United Kingdom UVB measurements and impacts review group*. HMSO.

Vachon, D., Lapierre, J. F., & del Giorgio, P. A. (2016). Seasonality of photochemical dissolved organic carbon mineralization and its relative contribution to pelagic CO2 production in northern lakes. *Journal of Geophysical Research: Biogeosciences*, *121*(3), 864–878. https://doi.org/10.1002/2015jg003244

Vernet, M. (2005). Effects of UV radiation on the physiology and ecology of marine phytoplankton. In S. De Mora, S. Demers, & M. Vernet (Eds.), *The effects of UV radiation in the marine environment* (pp. 237–278). Cambridge: Cambridge University Press.

Vernet, M., Neori, A., & Haxo, F. T. (1989). Spectral proprties and photosynthetic action in red-tide populations of *Prorocentrum micans* and *Gonyaulax polyedra*. *Marine Biology*, *103*(3), 365–371. https://doi.org/10.1007/bf00397271

Vernet, M., & Whitehead, K. (1996). Release of ultraviolet-absorbing compounds by the red-tide dinoflagellate Lingulodinium polyedra. *Marine Biology*, *127*(1), 35–44. https://doi.org/10.1007/bf00993641

Vigano, I., van Weelden, H., Holzinger, R., Keppler, F., McLeod, A., & Rockmann, T. (2008). Effect of UV radiation and temperature on the emission of methane from plant biomass and structural components. *Biogeosciences*, *5*(3), 937–947. https://doi.org/10.5194/bg-5-937-2008

Wang, Q.-W., Pieristè, M., Liu, C., Kenta, T., Robson, T. M., & Kurokawa, H. (2020). The contribution of photodegradation to litter decomposition in a temperate forest gap and understorey. *New Phytologist*, *229*(5), 2625–2636. https://doi.org/10.1111/nph.17022

Webb, A. R., Slaper, H., Koepke, P., & Schmalwieser, A. W. (2011). Know your standard: Clarifying the CIE Erythema Action Spectrum. *Photochemistry and Photobiology*, *87*(2), 483–486. https://doi.org/10.1111/j.1751-1097.2010.00871.x

Weiss, R. F., & Price, B. A. (1980). Nitrous oxide solubility in water and seawater. *Marine Chemistry*, *8*(4), 347–359. https://doi.org/10.1016/0304-4203(80)90024-9

White, E. M., Kieber, D. J., Sherrard, J., Miller, W. L., & Mopper, K. (2010). Carbon dioxide and carbon monoxide photoproduction quantum yields in the Delaware Estuary. *Marine Chemistry*, *118*(1–2), 11–21. https://doi.org/10.1016/j.marchem.2009.10.001

Wiesenburg, D. A., & Guinasso, N. L. Jr. (1979). Equilibrium solubilities of methane, carbon monoxide, and hydrogen in water and sea water. *Journal of Chemical & Engineering Data*, *24*(4), 356–360. https://doi.org/10.1021/je60083a006

Wilson, D. F., Swinnerton, J. W., & Lamontagne, R. A. (1970). Production of carbon monoxide and gaseous hydrocarbons in seawater - Relation to dissoplved organic carbon. *Science*, *168*(3939), 1577. https://doi.org/10.1126/science.168.3939.1577

Worldwide Weather Online (2019). *Oban Historical Weather*. Retrieved from https://www.worldweatheronline.com

Xie, H. X., & Zafiriou, O. C. (2009). Evidence for significant photochemical production of carbon monoxide by particles in coastal and oligotrophic marine waters. *Geophysical Research Letters*, *36*. https://doi.org/10.1029/2009gl041158

Xu, J. T., & Gao, K. S. (2016). Photosynthetic contribution of UV-A to carbon fixation by macroalgae. *Phycologia*, *55*(3), 318–322. https://doi.org/10.2216/15-91.1

Ye, W. W., Zhang, G. L., Li, P. P., Zhou, F., & Liu, C. G. (2019). Variations in dissolved methane in the Yellow Sea during the Spring algal blooms of 2009. *Journal of Ocean University of China*, *18*(4), 896–912. https://doi.org/10.1007/s11802-019-3993-4

Zaneveld, J. R. V. (1975). Penetration of ultraviolet radiation into natural waters. In D. S. Nachtwey, M. M. Caldwell, & R. H. Biggs (Eds.), *Impacts of climatic change on the biosphere. CIAP Monograph 5* (pp. 108–166). Washington, DC, USA: Climatic Impact Assessment Program, Department of Transportation.